Locally detecting UV cutoffs on a sphere with particle detectors

Ahmed Shalabi,[1,*] Laura J. Henderson,[2,1,†] and Robert B. Mann[1,3,4]

[1]*Department of Physics and Astronomy, University of Waterloo, Waterloo, Ontario, Canada, N2L 3G1*
[2]*Centre for Engineered Quantum Systems, School of Mathematics and Physics, The University of Queensland, Saint Lucia, Queensland 4072, Australia*
[3]*Institute for Quantum Computing, University of Waterloo, Waterloo, Ontario, Canada, N2L 3G1*
[4]*Perimeter Institute, 31 Caroline Street North, Waterloo, Ontario, Canada, N2L 2Y5*

(Received 15 November 2022; accepted 24 January 2023; published 13 February 2023)

The potential breakdown of the notion of a metric at high energy scales could imply the existence of a fundamental minimal length scale below which distances cannot be resolved. One approach to realizing this minimum length scale is to construct a quantum field theory with a bandlimit on the field. We report on an investigation of the effects of imposing a bandlimit on a field on a curved and compact spacetime and how best to detect such a bandlimit if it exists. To achieve this operationally, we couple two Gaussian-smeared Unruh-DeWitt detectors to a scalar field on a $S^2 \times R$ spherical spacetime through delta switching. The bandlimit is implemented through a cutoff of the allowable angular momentum modes of the field. We observe that a number of features of single detector response in the spherical case are similar to those in flat spacetime, including the dependence on the geometry of the detector, and that smaller detectors couple more strongly to the field, leading to an optimal size for bandlimit detection. We find that in flat spacetime squeezed detectors are more sensitive to the bandlimit provided they are larger than the optimal size; however, in spherical spacetime the bandlimit itself determines if squeezing improves the sensitivity. We also explore setups with two detectors, noting that in the spherical case, due to its compact nature, there is a lack of dissipation of any perturbation to the field, which results in locally excited signals being refocused at the poles. Quite strikingly, this feature can be exploited to significantly improve bandlimit detection via field mediated signaling. Moreover, we find that squeezing on a sphere introduces extra anisotropies that could be exploited to amplify or weaken the response of the second detector.

DOI: 10.1103/PhysRevD.107.045006

I. INTRODUCTION

The theories of general relativity and quantum field theory describe all fundamental interactions in nature. Yet they are based on entirely different mathematical structures and are empirically applicable over very different energy and length scales. While semiclassical descriptions of quantum field theory on curved spacetime exist, a fundamental step towards their unification into some higher energy theory of quantum gravity will entail understanding what happens at short distance scales. Fluctuations of quantum fields might potentially break down the notion of a general relativistic metric upon approaching the Planck scale. As such, it is believed that there is a finite minimum length beneath which distances cannot be resolved [1].

There are several consistent high energy theories of quantum gravity, each with its own treatment of spacetime. Generally, there are two overarching approaches to dealing with the nature of spacetime in theories of quantum gravity [2]. One is to model spacetime as some sort of discrete structure. This approach is conducive to quantization and would naturally entail some sort of ultraviolet (UV) cutoff. However it comes at the price of a loss of local Lorentzian symmetries. The other broad approach, based on continuous structures, does not suffer from these issues. However understanding the notion of metric breakdown remains an open problem [3].

In an attempt to reconcile these issues a hybrid proposal [4] treats spacetime as both continuous and discrete, analogous to the way that Shannon's sampling theorem [5] regards information as both continuous and discrete. More concretely, consider a continuous signal modeled by a function $f(t)$. Shannon's sampling theorem states that if $f(t)$ is bandlimited, i.e. contains frequencies in a finite interval $(-\Lambda, \Lambda)$, then taking a discrete set of samples $\{f(t_n)\}_{n=-\infty}^{n=\infty}$ is enough to reconstruct the signal via the Shannon sampling formula for all times, provided the samples are taken at intervals $t_{n+1} - t_n = 1/(2\Lambda)$. This was generalized to physical fields on Lorentzian manifolds, establishing how this form of bandlimitation on the momentum modes of a field is equivalent to a UV cutoff [6]. It is important to note

*ashalabi@uwaterloo.ca
†l7henderson@uwaterloo.ca

that, unlike quantizing a field on discrete lattice, bandlimitation of a quantum field theory preserves local Euclidean symmetries. Furthermore, although this form of bandlimitation is not Lorentz invariant, it can be generalized to a fully covariant cutoff [7,8].

With all of this established, it is of utmost importance to study UV cutoffs at the intersection between quantum field theory and general relativity—in other words, imposing a cutoff on a quantum field on a curved background. To this end, we here study this question on an $S^2 \times R$ spacetime and, for comparison, its $(2+1)$-dimensional Minkowski counterpart. We do so for several reasons. First, a quantized scalar field on an $S^2 \times R$ background has well defined angular momentum modes. Moreover, this spacetime is compact and bounded, so a quantized scalar field would have a countably infinite number of modes if no UV cutoff existed. Furthermore, AdS_3 is conformal to $S^2 \times R$, making our results straightforwardly transferrable to that context. AdS spacetimes have been studied extensively in the context of holographic duality and the AdS/CFT correspondence. In addition, the field correlation functions on AdS_3 are related to those in BTZ spacetimes via image sums [9].

The most straightforward way to probe quantum fields locally is through particle detectors. First proposed by Unruh [10], the detector is modeled as a two-level system that (linearly) couples to the field. As such, it serves as a local probe of the field, providing both a concrete notion of locality and an operational definition of a particle. In other words, "A particle is what a particle detector detects" [11].

Particle detectors probe and study the semiclassical regime of quantum field theory on curved spacetime. They sample the fluctuations and (if more than one detector is employed) correlations of a quantum field by coupling to its momentum modes. By smearing a particle detector over a region of spacetime, we can probe the quantum field in question via local interactions over that region. Since the field degrees of freedom and the spatial profile of the detector (which quantifies where the detector couples to the field) enter the model at the same level, an investigation of how they interact can yield a better operational understanding of the finite spatial volume of the discrete degrees of freedom. Such a study was recently carried out in $(3+1)$-dimensional flat spacetime [12]. Here we take the next natural step by considering this problem in $S^2 \times R$, with appropriate comparison to $(2+1)$-dimensional flat spacetime.

There are several models for the field-detector coupling. These include nonlinear scalar field coupling [13], field derivative coupling [14,15], fermionic couplings [16,17] and delocalized matter [18,19]. However, a simple linear coupling [20] is an appropriate approximation to the full light-matter interaction if angular momentum exchange is negligible [21,22]. We shall only consider this coupling in our investigation.

Particle detector models have found many applications in the study of quantum information in both flat and curved spacetimes. These include studies of the entanglement structure of quantum fields using the entanglement harvesting protocol [20,23], the Unruh effect [24], Hawking radiation [25], probing the geometry [26,27] and topology [28] of spacetime, providing a measurement framework for quantum field theory [29], and other applications like communication protocols [30,31] and thermodynamics [32].

We consider here the question of how to best detect the presence of a cutoff using particle detectors in both flat and curved spacetimes. We utilize particle detectors by coupling them to vacuum states of quantum fields in each of $(2+1)$-dimensional Minkowski spacetime and on $S^2 \times R$ as a prototypical $(2+1)$-dimensional curved spacetime. We will implement the UV cutoffs via a hard/conventional bandlimitation on the momentum modes of the scalar field. We will take the field-detector coupling duration to be the shortest length scale in the problem by modeling it as a δ function. This delta coupling has several advantages. It removes the need for time ordering and allows a full nonperturbative determination of the final detector-field joint state [33]. After the field is traced out, the final state of the detector carries information about the geometry of the underlying spacetime [27]. Furthermore, as discussed earlier, although the conventional bandlimit is not covariant, we expect our results to be similar to a full covariant generalization since the duration of the coupling we employ is smaller than any other length scales in the problem. Finally, we will use two detectors, switching on one before the other to study the impact of field mediated signaling on the detection of the bandlimit.

The rest of the paper is organized as follows. In Sec. II we present the basic formalism of the Unruh-DeWitt (UDW) model in the context of δ switching and bandlimited quantum fields for both the flat and spherical cases we consider, and in Sec. III we describe the spatial profiles of the detectors. We then present our results for bandlimit detection using a single detector in Sec. IV and for two detectors in Sec. V A. We present our conclusions in Sec. VI along with a discussion of directions for further work. A set of Appendices contains technical details pertinent to our investigation.

II. THE UDW DETECTOR MODEL AND DIRAC δ SWITCHING

The Unruh-DeWitt (UDW) detector [10,34,35] is a two-level system whose ground and excited states are respectively given by $|g\rangle_D$ and $|e\rangle_D$, separated by an energy gap Ω_D. We shall consider two such detectors A and B linearly coupled to a massless scalar field such that the initial joint detector-field state is given by

$$\hat{\rho}_i = |g\rangle_{AA}\langle g| \otimes |g\rangle_{BB}\langle g| \otimes |0\rangle_{\phi\phi}\langle 0| \tag{1}$$

or in other words, the field is in the vacuum state and the detectors are in their ground states. The interaction detector-field Hamiltonian is

$$\hat{H}_{I,AB}(t) = \hat{H}_{I,A}(t) + \hat{H}_{I,B}(t) \tag{2}$$

in the interaction picture, where $\hat{H}_{I,D}(t)$ is given by

$$\hat{H}_{I,D}(t) = \lambda_D \chi_D(t)(\mathrm{e}^{\mathrm{i}\Omega_D t}\hat{\sigma}_D^+ + \mathrm{e}^{-\mathrm{i}\Omega_D t}\hat{\sigma}_D^-) \otimes \int d^n\boldsymbol{x} F_D(\boldsymbol{x}-\boldsymbol{x}_D)\hat{\phi}(\boldsymbol{x},t) \tag{3}$$

with $D \in \{A, B\}$, where λ_D is the field-detector coupling constant and $\chi_D(t)$ is the switching function that controls the duration of the field-detector interaction. The operators $\hat{\sigma}_D^+ \coloneqq |e\rangle_{DD}\langle g|$ and $\hat{\sigma}_D^- \coloneqq |g\rangle_{DD}\langle e|$ are the SU(2) ladder operators acting on the Hilbert space of detector D. We have introduced a spatial profile $F_D(\boldsymbol{x}-\boldsymbol{x}_D)$ for each detector, centered around its position $\boldsymbol{x}_D$. We interpret this as describing the size and shape of the detector [36,37].

The time evolution of the full detector-field system is

$$\hat{U} = \mathcal{T}\exp\left[-\mathrm{i}\int_{-\infty}^{\infty} \mathrm{d}t \hat{H}_{\mathrm{I},AB}(t)\right], \tag{4}$$

where $\mathcal{T}$ is the time ordering operator. The final state of the two detector-field system is given by

$$\hat{\rho}_f = \hat{U}\hat{\rho}_i\hat{U}^\dagger \tag{5}$$

in turn yielding the reduced density matrix describing the final state of the two detector system,

$$\hat{\rho}_{AB} \coloneqq \mathrm{Tr}_\phi[\hat{\rho}_f], \tag{6}$$

obtained by tracing out the Hilbert space of the field.

The general approach from here would be to solve for the matrix elements of $\hat{\rho}_{AB}$ perturbatively. However, it is possible to solve the two detector density matrix exactly [33,38] by using the switching function

$$\chi_D(t) = \eta_D \delta(t - T_D), \tag{7}$$

where T_D is the time at which the interaction takes place. We shall briefly review this "δ-switching" formalism without imposing the original constraint [33] of working in Minkowski space.

We will assume without loss of generality that detector A switches before B ($T_A \leq T_B$). Applying the δ switching allows us to write the time evolution operator (4) as

$$\hat{U}_\delta = \exp(\hat{H}_{I,B}(T_B))\exp(\hat{H}_{I,A}(T_A)) \tag{8}$$

or alternatively as

$$\hat{U}_\delta = \exp(\hat{\mu}_B(T_B)\otimes\hat{\mathcal{Y}}_B)\exp(\hat{\mu}_A(T_A)\otimes\hat{\mathcal{Y}}_A), \tag{9}$$

where the operator

$$\hat{\mu}_D(t) = \mathrm{e}^{\mathrm{i}\Omega_D\tau_D(t)}\hat{\sigma}_D^+ + \mathrm{e}^{-\mathrm{i}\Omega_D\tau_D(t)}\hat{\sigma}_D^- \tag{10}$$

describes the evolution of the detector and

$$\hat{\mathcal{Y}}_D \coloneqq -\mathrm{i}\lambda_D\eta_D\int d^n\boldsymbol{x} F_D(\boldsymbol{x}-\boldsymbol{x}_D)\hat{\phi}(\boldsymbol{x},T_D) \tag{11}$$

which is the smeared field operator.

By expanding the Taylor series of the exponential and noting that $\hat{\mu}_D(t)^2 = \mathbb{1}$, we can write the time evolution operator $\hat{U}_\delta$ as

$$\hat{U}_\delta = (\mathbb{1}_A\otimes\mathbb{1}_B\otimes\cosh(\hat{\mathcal{Y}}_B) + \mathbb{1}_A\otimes\hat{\mu}_B(T_B)\otimes\sinh(\hat{\mathcal{Y}}_B)) \times (\mathbb{1}_A\otimes\mathbb{1}_B\otimes\cosh(\hat{\mathcal{Y}}_A) + \hat{\mu}_A(T_A)\otimes\mathbb{1}_B\otimes\sinh(\hat{\mathcal{Y}}_A)). \tag{12}$$

Moreover, we can rewrite $\hat{U}_\delta$ using the complex exponential form of the hyperbolic trigonometric functions utilizing the following definition. Let $j, k \in \{1, -1\}$ and write

$$\hat{X}_{(j,k)} = \frac{1}{4}(e^{\hat{\mathcal{Y}}_B} + je^{-\hat{\mathcal{Y}}_B})(e^{\hat{\mathcal{Y}}_A} + ke^{-\hat{\mathcal{Y}}_A}) \tag{13}$$

which gives

$$\hat{U}_\delta = \mathbb{1}_A\otimes\mathbb{1}_B\otimes\hat{X}_{(1,1)} + \hat{\mu}_A(T_A)\otimes\hat{\mu}_B(T_B)\otimes\hat{X}_{(-1,-1)} + \hat{\mu}_A(T_A)\otimes\mathbb{1}_B\otimes\hat{X}_{(1,-1)} + \mathbb{1}_A\otimes\hat{\mu}_B(T_B)\otimes\hat{X}_{(-1,1)} \tag{14}$$

from (12). The two detector subsystem evolves to the final state

$$\hat{\rho}_{AB} = \mathrm{Tr}_\phi[\hat{U}_\delta\hat{\rho}_i\hat{U}_\delta^\dagger] \tag{15}$$

which in the $|a\rangle_A\otimes|b\rangle_B$ basis for $a, b \in \{g, e\}$ contains cross terms of the form $\langle 0|\hat{X}_{(j,k)}\hat{X}_{(l,m)}|0\rangle$. This motivates the following definition:

$$f_{jklm} \coloneqq \langle 0|\hat{X}_{(j,k)}^\dagger\hat{X}_{(l,m)}|0\rangle, \tag{16}$$

where $j, k, l, m \in \{1, -1\}$. Using the Baker-Campbell-Hausdorff (BCH) formula $e^Xe^Y = e^Z$ with Z given by

$$Z = X + Y + \frac{1}{2}[X,Y] + \frac{1}{12}[X,[X,Y]] - \frac{1}{12}[Y,[X,Y]] + \cdots \tag{17}$$

and using arguments similar to those in the Minkowski space case [33], we rewrite the f_{jklm} matrix elements as

$$f_{jklm} = \frac{1}{16}[(1 + j\ell + km + jk\ell m) + [(1 + j\ell)(k + m)]f_A + [(\ell + jkm)e^{2i\Theta} + (j + k\ell m)e^{-2i\Theta}]f_B + [(jk + \ell m)e^{\omega} + (jm + k\ell)e^{-\omega}]f_A f_B], \tag{18}$$

where

$$f_D = \langle 0|\exp(2\hat{\mathcal{Y}}_D)|0\rangle \tag{19}$$

and the quantities Θ and ω are defined as

$$\Theta := -i\langle 0|[\mathcal{Y}_A, \hat{\mathcal{Y}}_B]|0\rangle = \langle 0|\hat{\Theta}|0\rangle$$
$$\omega := 2\langle 0|\{\hat{\mathcal{Y}}_A, \hat{\mathcal{Y}}_B\}|0\rangle = \langle 0|\hat{\omega}|0\rangle \tag{20}$$

which are respectively the vacuum expectation values of the smeared field commutator and anticommutator. For two regions in a spacetime, these operators encode the signaling through the field and the correlations in the field between the two regions.

The smeared field commutator Θ is nonzero when two smeared detectors are in casual contact, in which case communication between them is possible. It is zero when the detectors are spacelike separated. It is important to note that for two detectors that are initially separable there is no dependence of the final state on ω after the interaction. This is to be expected since ω encodes the amount of correlations between two detectors—if they are uncorrelated initially then they cannot harvest entanglement from the field via delta coupling [33,39]. The role played by the anticommutator ω in detector correlations with delta coupling was recently studied [39]. We will analyze in Sec. IV A the relevance of Θ in signaling.

The final reduced density matrix $\hat{\rho}_{AB}$ can then be written in terms of the $f_{jk\ell m}$ matrix elements as

$$\hat{\rho}_{AB} = \begin{pmatrix} \rho_{11} & 0 & 0 & \rho_{14} \\ 0 & \rho_{22} & \rho_{23} & 0 \\ 0 & \rho_{23}^* & \rho_{33} & 0 \\ \rho_{14}^* & 0 & 0 & \rho_{44} \end{pmatrix}, \tag{21}$$

where the nonzero ρ_{ij} matrix elements are given by

$$\rho_{11} = \frac{1}{4}(1 + f_A + f_B\cos(2\Theta) + f_A f_B\cosh(\omega)) \tag{22a}$$

$$\rho_{14} = \frac{1}{4}e^{-i(\Omega_A T_A + \Omega_B T_B)} f_B(i\sin(2\Theta) + f_A\sinh(\omega)) \tag{22b}$$

$$\rho_{22} = \frac{1}{4}(1 + f_A - f_B\cos(2\Theta) - f_A f_B\cosh(\omega)) \tag{22c}$$

$$\rho_{23} = -\frac{1}{4}e^{-i(\Omega_A T_A - \Omega_B T_B)} f_B(i\sin(2\Theta) + f_A\sinh(\omega)) \tag{22d}$$

$$\rho_{33} = \frac{1}{4}(1 - f_A + f_B\cos(2\Theta) - f_A f_B\cosh(\omega)) \tag{22e}$$

$$\rho_{44} = \frac{1}{4}(1 - f_A - f_B\cos(2\Theta) + f_A f_B\cosh(\omega)). \tag{22f}$$

We can also trace out the detectors individually to obtain the following density operators:

$$\hat{\rho}_A = \mathrm{Tr}_B[\hat{\rho}_{AB}] = \frac{1}{2}\begin{pmatrix} 1 + f_A & 0 \\ 0 & 1 - f_A \end{pmatrix} \tag{23}$$

and

$$\hat{\rho}_B = \mathrm{Tr}_A[\hat{\rho}_{AB}] = \frac{1}{2}\begin{pmatrix} 1 + f_B\cos(2\Theta) & 0 \\ 0 & 1 - f_B\cos(2\Theta) \end{pmatrix}. \tag{24}$$

Note that the dynamics of detector B is modified by the commutator of the field. This is a consequence of the fact that detector B interacts with an evolved state of the field subsequent to its interaction with the first detector. Finally, we can read off the transition probabilities for the first and second detector to be

$$P_A = \frac{1}{2}(1 - f_A) \quad \text{and} \quad P_B = \frac{1}{2}(1 - f_B\cos(2\Theta)). \tag{25}$$

The dynamics and the response of δ-coupled detectors can be extended to those on any curved spacetime by quantizing the scalar field on the background spacetime. The Klein-Gordon equation in curved spacetime is

$$\left(\frac{1}{\sqrt{|g|}}\frac{\partial}{\partial x^\mu} g^{\mu\nu}\sqrt{|g|}\frac{\partial}{\partial x^\nu}\right)\hat{\phi}(x,t) = 0. \tag{26}$$

We can solve the Klein-Gordon equation by assuming the following ansatz for the scalar field operator:

$$\hat{\phi}(x,t) = \sum_k [u_k(x,t)\hat{a}_k + u_k(x,t)^*\hat{a}_k^\dagger], \tag{27}$$

where the functions $u_k(x,t)$ are solutions to the Klein-Gordon equation, and $\hat{a}_k$, $\hat{a}_k^\dagger$ are the raising and lowering operators of the scalar field. If the spacetime is globally hyperbolic, then a set of modes $u_k(x,t)$ exists. If we can quantize the scalar field on some background spacetime, the task would be to derive the smeared field operator $\hat{\mathcal{Y}}_D$ and from it the expressions for f_D and Θ that define the response of the two detectors to the coupling. Moreover, we can particularize those expressions to the shape and localization of the detectors on the background geometry.

A. Flat spacetime

Here we briefly summarize the recent $(3+1)$-dimensional flat space analysis [12] in a $(2+1)$-dimensional context for ease of comparison with the spherical case. We decompose the scalar field into plane-wave modes as

$$\hat{\phi}(\boldsymbol{x},t)=\frac{1}{(2\pi)^{n/2}}\int\frac{d^2\boldsymbol{k}}{\sqrt{2|\boldsymbol{k}|}}[e^{i(|\boldsymbol{k}|t-\boldsymbol{k}\cdot\boldsymbol{x})}\hat{a}_{\boldsymbol{k}}^{\dagger}+\text{H.c.}], \tag{28}$$

where $\hat{a}_{\boldsymbol{k}}^{\dagger}$, $\hat{a}_{\boldsymbol{k}}$ are creation and annihilation operators that obey the canonical commutation relations

$$[\hat{a}_{\boldsymbol{k}},\hat{a}_{\boldsymbol{k}'}^{\dagger}]=\delta^{(2)}(\boldsymbol{k}-\boldsymbol{k}'). \tag{29}$$

After writing down the field, we can now calculate the density matrix describing the joint state of the two detector system (21). In the case of $(2+1)$-dimensional Minkowski space, the smeared field operator is

$$\hat{\mathcal{Y}}_D=-i\lambda_D\eta_D\int\frac{d^2\boldsymbol{k}}{\sqrt{2|\boldsymbol{k}|}}(\tilde{F}_D(\boldsymbol{k})e^{-i(|\boldsymbol{k}|T_D-\boldsymbol{k}\cdot x_D)}\hat{a}_{\boldsymbol{k}}+\text{H.c.}), \tag{30}$$

where

$$\tilde{F}_D(\boldsymbol{k})=\frac{1}{2\pi}\int d^2\boldsymbol{x}F_D(\boldsymbol{x})e^{i\boldsymbol{k}\cdot\boldsymbol{x}} \tag{31}$$

is the Fourier transform of the spatial profile.

It is straightforward to calculate the matrix element functions (19) and (20) as [33]

$$\begin{aligned}
f_D&=\exp\left(-\lambda_D^2\eta_D^2\int_{|\boldsymbol{k}|<\Lambda}\frac{d^2\boldsymbol{k}}{|\boldsymbol{k}|}|\tilde{F}_D(\boldsymbol{k})|^2\right)\\
\Theta&=-\frac{i\lambda_A\lambda_B\eta_A\eta_B}{2}\int_{|\boldsymbol{k}|<\Lambda}\frac{d^2\boldsymbol{k}}{|\boldsymbol{k}|}(\tilde{F}_A^{*}(\boldsymbol{k})\tilde{F}_B(\boldsymbol{k})e^{-i|\boldsymbol{k}|(T_B-T_A)}e^{i\boldsymbol{k}\cdot(\boldsymbol{x}_B-\boldsymbol{x}_A)}-\text{H.c.})\\
\omega&=\lambda_A\lambda_B\eta_A\eta_B\int_{|\boldsymbol{k}|<\Lambda}\frac{d^2\boldsymbol{k}}{|\boldsymbol{k}|}(\tilde{F}_A^{*}(\boldsymbol{k})\tilde{F}_B(\boldsymbol{k})e^{-i|\boldsymbol{k}|(T_B-T_A)}e^{i\boldsymbol{k}\cdot(\boldsymbol{x}_B-\boldsymbol{x}_A)}+\text{H.c.}).
\end{aligned} \tag{32}$$

Expanding the field in the plane-wave modes of Eq. (28), we are able to easily introduce a hard momentum cutoff by removing modes where $|\boldsymbol{k}|>\Lambda$ [12]. We note that this cutoff is not Lorentz invariant, but expect that results will be similar to the case of the full covariant cutoff, since the switching time of the detector is shorter than any other scale in the problem [7,8].

B. Spherical spacetime

To generalize δ switching to the spherical spacetime we will need to quantize the scalar field $\hat{\phi}$ and derive from it the smeared field operator $\hat{\mathcal{Y}}_D$ for each detector. We shall then obtain expressions for f_D that define the transition probability P_D for each detector. We shall also need an expression for the commutator Θ of the smeared field operators to obtain the transition probability of the second detector after it has interacted with the evolved state of the field.

Quantizing a conformally coupled scalar field on $\mathbb{R}\times\mathbb{S}^2$ was done in [40]. From the metric

$$ds^2=-dt^2+d\theta^2+\sin^2(\theta)d\varphi^2, \tag{33}$$

where $-\infty<t<\infty$, $0<\theta<\pi$ and $0<\varphi<2\pi$, the Klein-Gordon equation then becomes

$$\Box\psi-\frac{1}{8}R\psi=0, \tag{34}$$

whose solutions are given by

$$\psi_{\ell m}=\frac{1}{\sqrt{2\ell+1}}e^{-i(\ell+\frac{1}{2})t}Y_{\ell m}(\theta,\varphi), \tag{35}$$

where

$$Y_{\ell m}(\theta,\varphi)=(-1)^m N_{\ell m}P_{\ell}^{m}(\cos\theta)e^{im\varphi} \tag{36}$$

are the spherical harmonics basis functions, P_{ℓ}^{m} are associated Legendre polynomials and

$$N_{\ell m}\equiv\sqrt{\frac{(2\ell+1)}{4\pi}\frac{(\ell-m)!}{(\ell+m)!}}. \tag{37}$$

This allows us to expand the scalar field $\hat{\phi}$ in the modes $\psi_{\ell m}$ as follows:

$$\hat{\phi}=\sum_{\ell,m}\psi_{\ell m}\hat{a}_{\ell m}+\psi_{\ell m}^{*}\hat{a}_{\ell m}^{\dagger}, \tag{38}$$

where $\hat{a}_{\ell m}$ and $\hat{a}_{\ell m}^{\dagger}$ are creation and annihilation operators such that $\hat{a}_{\ell m}^{\dagger}|0\rangle=|\ell,m\rangle$, and where

$$[\hat{a}_{ij}^{\dagger},\hat{a}_{\ell m}]=\delta_{i\ell}\delta_{jm}. \tag{39}$$

That is, $\hat{a}_{\ell m}$ and $\hat{a}^\dagger_{\ell m}$ raise and lower the angular momentum of the scalar field. We can expand any function on $\mathbb{S}^2$ in terms of spherical harmonics as

$$h(\theta,\varphi) = \sum_{l,m} h_{lm} Y_{lm}(\theta,\varphi) \tag{40}$$

and using the orthogonality condition

$$\int\int \mathrm{d}\theta \mathrm{d}\varphi \, \sin(\theta) Y_{\ell m}(\theta,\varphi) Y^*_{pq}(\theta,\varphi) = \delta_{mq}\delta_{pl} \tag{41}$$

we can compute the coefficients

$$h_{lm} = \int\int \mathrm{d}\theta \mathrm{d}\varphi \sin(\theta) h(\theta,\varphi) Y^*_{\ell m}(\theta,\varphi) \tag{42}$$

in (40).

Expanding the smeared field operator in terms of the scalar field modes we get

$$\hat{\mathcal{Y}}_D = -\mathrm{i}\lambda_D \eta_D \int \mathrm{d}\Omega F_D(\boldsymbol{\theta} - \boldsymbol{\theta}_D)\left(\sum_{\ell,m} \psi_{\ell m}\hat{a}_{\ell m} + \psi_{\ell m}\hat{a}^\dagger_{\ell m}\right), \tag{43}$$

where $\int \mathrm{d}\Omega \coloneqq \int\int \mathrm{d}\theta \mathrm{d}\varphi \sin(\theta)$ for a profile $F(\boldsymbol{\theta})$ centered at $\boldsymbol{\theta}_D = (\theta_D, \varphi_D)$. Expressing the spatial localization function in the spherical harmonics basis, with $F_D = \sum_{p,q} f_{pq} Y_{pq}$ we obtain

$$\hat{\mathcal{Y}}_D = -\mathrm{i}\lambda_D \eta_D \int \mathrm{d}\Omega \sum_{p,q} f_{pq} Y_{pq}(\theta,\varphi) \sum_{l,m} (\psi_{\ell m}\hat{a}_{\ell m} + \psi_{\ell m}\hat{a}^\dagger_{lm}) \tag{44}$$

for the smeared field operator. Writing $\hat{\mathcal{Y}}_D \coloneqq \hat{y} + \hat{y}^*$ we have

$$\begin{aligned}
\hat{y}^* &= -\mathrm{i}\lambda_D \eta_D \int \mathrm{d}\Omega \sum_{p,q} f_{pq} Y_{pq}(\theta,\varphi) \sum_{l,m} \psi_{\ell m}\hat{a}^\dagger_{lm} \\
&= -\mathrm{i}\lambda_D \eta_D \sum_{l,m}\sum_{p,q} \frac{e^{i(\ell+\frac{1}{2})T_D} f_{pq}}{\sqrt{(2\ell+1)}} \int \mathrm{d}\Omega Y_{pq}(\theta,\varphi) Y^*_{lm} \hat{a}^\dagger_{lm} \\
&= -\mathrm{i}\lambda_D \eta_D \sum_{l,m} \frac{1}{\sqrt{(2\ell+1)}} e^{i(\ell+\frac{1}{2})T_D} f_{\ell m}\hat{a}^\dagger_{lm}
\end{aligned} \tag{45}$$

using (35) and the orthogonality condition of the spherical harmonics.

For the $\hat{y}$ term a similar argument gives

$$\hat{y} = +\mathrm{i}\lambda_D \eta_D \sum_{l,m} \frac{1}{\sqrt{2\ell+1}} e^{-i(\ell+\frac{1}{2})T_D} f^*_{\ell m}\hat{a}_{lm} \tag{46}$$

so that

$$\begin{aligned}
\hat{\mathcal{Y}}_D &= \sum_{l,m} \frac{-\mathrm{i}\lambda_D \eta_D}{\sqrt{(2\ell+1)}} (e^{\mathrm{i}(\ell+\frac{1}{2})t_D} f_{\ell m}\hat{a}^\dagger_{lm} + e^{-\mathrm{i}(\ell+\frac{1}{2})t_D} f^*_{\ell m}\hat{a}_{lm}) \\
&= \sum_{\ell,m} (\alpha_{\ell m}\hat{a}^\dagger_{\ell m} - \alpha^*_{\ell m}\hat{a}_{\ell m})
\end{aligned} \tag{47}$$

with $\alpha_{\ell m}$ defined as

$$\alpha_{\ell m} \coloneqq -\frac{\mathrm{i}\lambda_D \eta_D}{\sqrt{2\ell+1}} e^{i(\ell+\frac{1}{2})T_D} f_{\ell m}. \tag{48}$$

Analogous to the case in Minkowski space [33], the exponential of the smeared field operator acts on the vacuum state, resulting in a state that corresponds to the phase space displacement of the vacuum state

$$\hat{\mathcal{D}}_{\ell m}|0\rangle = \mathrm{e}^{\hat{\mathcal{Y}}_D}|0\rangle = |\alpha_{\ell m}\rangle \tag{49}$$

due to the interaction with the detector. The displaced state is indeed a coherent state, since it is an eigenstate of the annihilation operator

$$\hat{a}_{ij}|\alpha_{\ell m}\rangle = \alpha_{ij}|\alpha_{\ell m}\rangle \tag{50}$$

as shown in Appendix A. To compute $f_D = \langle 0|\exp^{2\hat{\mathcal{Y}}_D}|0\rangle$ we begin by computing the Taylor series for the exponential of the smeared field operator. The computation follows as a special case of the proof presented in Appendix A of [33] due to the linearity of sums:

$$\begin{aligned}
f_D &= \langle 0|\exp\sum_{\ell,m} 2(\alpha_{\ell m}\hat{a}^\dagger_{\ell m} - \alpha^*_{\ell m}\hat{a}_{\ell m})|0\rangle \\
&= \langle 0|0\rangle + \sum_{\ell,m} 2\langle 0|\cancel{\alpha_{\ell m}\hat{a}^\dagger_{\ell m}} - \cancel{\alpha^*_{\ell m}\hat{a}_{\ell m}}|0\rangle + \frac{2}{2!}\sum_{\ell,m}\sum_{\ell',m'}\langle 0|(\cancel{\alpha_{\ell m}\hat{a}^\dagger_{\ell m}} - \alpha^*_{\ell m}\hat{a}_{\ell m})(\alpha_{\ell' m'}\hat{a}^\dagger_{\ell' m'} - \cancel{\alpha^*_{\ell' m'}\hat{a}_{\ell' m'}})|0\rangle + \cdots \\
&= 1 + 0 - \sum_{\ell,m}\sum_{\ell',m'}\langle \ell', m'|\ell, m\rangle \alpha_{\ell' m'}\alpha^*_{\ell m} + \cdots.
\end{aligned} \tag{51}$$

The orthogonality relation implies that $\langle \ell, m|\ell', m'\rangle = \delta_{\ell\ell'}\delta_{mm'}$. Moreover, each term in the sum containing an odd number of creation and annihilation operators vanishes by Wick's theorem, i.e.

$$\langle 0|(\alpha_j \hat{a}_j^\dagger - \alpha_j^* \hat{a}_j)^{(2n+1)}|0\rangle = 0 \tag{52}$$

in general. The even terms recombine [33], yielding

$$f_D = \exp\left(-\sum_{\ell=0}^{\infty}\sum_{m=-\ell}^{\ell}|\alpha_{\ell m}^D|^2\right). \tag{53}$$

Finally, using (47) and the commutation relations (39), we find

$$\begin{aligned}\Theta = -\mathrm{i}[\hat{\mathcal{Y}}_A, \hat{\mathcal{Y}}_B] &= \mathrm{i}\lambda_A\lambda_B\eta_A\eta_B\left[\sum_{\ell,m}\frac{1}{\sqrt{2\ell+1}}\sum_{i,j}\frac{1}{\sqrt{2i+1}} f^{A}_{\ell,m}{}^{*} f^{B}_{i,j}\mathrm{e}^{-\mathrm{i}(\ell+1/2)T_A}\mathrm{e}^{\mathrm{i}(i+1/2)T_B}(\hat{a}_{\ell,m}\hat{a}^\dagger_{i,j} - \hat{a}^\dagger_{i,j}\hat{a}_{\ell,m})\right.\\ &\left. + f^{A}_{\ell,m} f^{B}_{i,j}{}^{*}\mathrm{e}^{\mathrm{i}(\ell+1/2)T_A}\mathrm{e}^{-\mathrm{i}(i+1/2)T_B}(\hat{a}^\dagger_{\ell,m}\hat{a}_{i,j} - \hat{a}_{i,j}\hat{a}^\dagger_{\ell,m})\right]\\ &= \mathrm{i}\lambda_A\lambda_B\eta_A\eta_B\sum_{\ell,m}\frac{1}{2\ell+1}[f^{A*}_{\ell,m} f^{B}_{\ell,m}\mathrm{e}^{\mathrm{i}(\ell+1/2)(T_B-T_A)} - f^{A}_{\ell,m} f^{B*}_{\ell,m}\mathrm{e}^{-\mathrm{i}(\ell+1/2)(T_B-T_A)}].\end{aligned} \tag{54}$$

Similar to the Minkowski spacetime bandlimit, the hard cutoff is implemented by removing all modes with $\ell > \ell_{\max}$. This is a straightforward extension of the flat space cutoff to $S^2 \times R$, since it is a cutoff of the conjugate momentum degrees of freedom to θ and φ. The same argument as to why we would not expect artifacts due to the noncovariant nature of the cutoff applies here as well. Finally, as was discussed in [12], the impact of the bandlimit can also be viewed as a nonlocal profile in the absence of a bandlimit since if we were to expand the profile in spherical harmonics

$$\begin{aligned}\sum_{\ell=0}^{\ell_{\max}}\sum_{m=-\ell}^{m=\ell} f_{\ell m}Y_{\ell m} &= \sum_{\ell=0}^{\infty}\sum_{m=-\ell}^{m=\ell} h_\ell f_{\ell m}Y_{\ell m}\\ &= \sum_{\ell=0}^{\infty}\sum_{m=-\ell}^{m=\ell}\tilde{f}_{\ell m}Y_{\ell m},\end{aligned} \tag{55}$$

where h_ℓ is 1 for $\ell \le \ell_{\max}$ and 0 otherwise. The $\tilde{f}_{\ell m}$ coefficients correspond to the equivalent nonlocal profile in the absence of a bandlimit. Figure 1 shows that the bandlimit leads to a detector profile that is highly nonlocal.

III. SETUP

Throughout the rest of this paper, we will take the two UDW detectors to couple to the field with the same interaction strength $\lambda_A = \lambda_B = \lambda$ and to have identical switching functions $\eta_A = \eta_B = \eta$. We will also take the spatial profile of the detectors to be two-dimensional normal or Gaussian distribution profiles, henceforth referred to as Gaussian detectors. We choose Gaussian detectors to maintain consistency with many previous studies in relativistic quantum information; our analysis can be extended to other types of spatial profile straightforwardly.

A. Flat spacetime

In $(2+1)$-dimensional Minkowski spacetime, a Gaussian detector has the spatial profile

$$F(x,y) = \frac{1}{2\pi ab}\exp\left(-\frac{x^2}{2a^2}\right)\exp\left(-\frac{y^2}{2b^2}\right), \tag{56}$$

where a describes the width in the x direction and b describes the width in the y direction. We note that decreasing the values of a and b decreases the size of the detector. It is convenient to rewrite the profile in polar coordinates as

$$F(r,\vartheta) = \frac{\sqrt{1-\epsilon^2}}{2\pi b^2}\exp\left(-\frac{r^2}{2b^2}(1-\epsilon^2\cos^2(\vartheta))\right), \tag{57}$$

where

$$\epsilon := \sqrt{1-\frac{b^2}{a^2}} \in [0,1) \tag{58}$$

describes the eccentricity of the Gaussian, with higher values of ϵ denoting larger squeezing. For completeness, we write down the Fourier transform of the spatial profile:

$$\tilde{F}(k,\theta) = \frac{1}{2\pi}\exp\left(-\frac{a^2|\boldsymbol{k}|^2}{2}(1-\epsilon^2\sin^2(\theta))\right). \tag{59}$$

By introducing a nonzero eccentricity to the spatial profile, we will be able to rotate the semimajor axes of the detectors away from the x axis of the chosen coordinate system by some angle, φ_D. Since the rotation operator commutes with the Fourier transform, the rotation can be easily implemented by taking $\theta \to \theta - \varphi_D$ in Eq. (59).

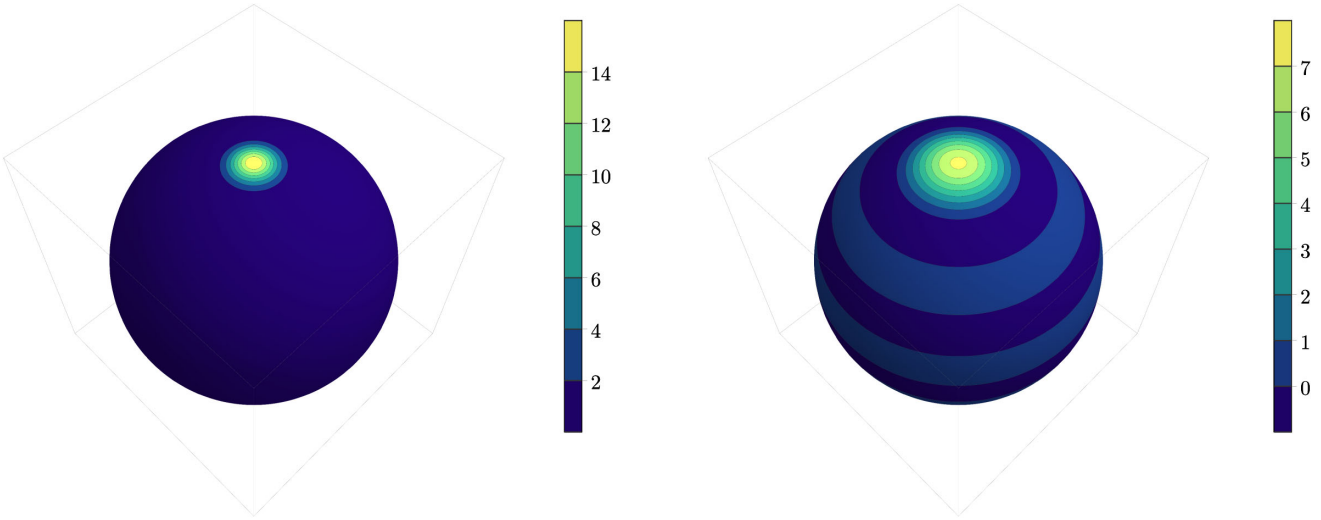

FIG. 1. Left: the spherical analog of a Gaussian distribution, the Fisher-Bingham five-parameter (FB5) distribution, with a size of $\kappa = 100$ and zero squeezing ($\beta = 0$) [Eq. (75)]. Right: the same FB5 distribution with $\kappa = 100$ and $\beta = 0$, approximately reconstructed in the spherical harmonic basis [Eq. (40)] with a cutoff of $\ell_{\rm Max} = 10$. When the cutoff is not present, the distribution is highly localized at the north pole, but when the cutoff is present, the distribution has support over the entire sphere.

With the spatial profile of the two detectors given, we are able to write down the expressions for the basic quantities that compose the matrix element functions:

$$f_D = \exp\left(-\frac{\lambda_D^2\eta_D^2}{8\pi^{3/2}a_D}\int_0^{2\pi} d\theta \frac{\mathrm{erf}(\Lambda a_D\sqrt{1-\epsilon_D^2\sin^2(\theta)})}{\sqrt{1-\epsilon_D^2\sin^2(\theta)}}\right) \tag{60}$$

$$\Theta = \frac{\lambda_A\lambda_B\eta_A\eta_B}{4\sqrt{2}\pi^{3/2}}\int_0^{2\pi} d\theta \frac{\exp\left(-\frac{[T-S\cos(\theta)]^2}{2\mathcal{A}(\theta)}\right)}{\sqrt{\mathcal{A}(\theta)}}\left\{\mathrm{Re}\left[\mathrm{erfi}\left(\frac{T-S\cos(\theta)}{\sqrt{2\mathcal{A}(\theta)}}+\frac{i\Lambda\sqrt{\mathcal{A}(\theta)}}{\sqrt{2}}\right)\right]-\mathrm{erfi}\left(\frac{T-S\cos(\theta)}{\sqrt{2\mathcal{A}(\theta)}}\right)\right\} \tag{61}$$

$$\omega = \frac{\lambda_A\lambda_B\eta_A\eta_B}{(2\pi)^{3/2}}\int_0^{2\pi} d\theta \frac{\exp\left(-\frac{[T-S\cos(\theta)]^2}{2\mathcal{A}(\theta)}\right)}{\sqrt{\mathcal{A}(\theta)}}\mathrm{Im}\left[\mathrm{erfi}\left(\frac{T-S\cos(\theta)}{\sqrt{2\mathcal{A}(\theta)}}+\frac{i\Lambda\sqrt{\mathcal{A}(\theta)}}{\sqrt{2}}\right)\right], \tag{62}$$

where we define $T \coloneqq T_B - T_A$, $S \coloneqq |\boldsymbol{x}_B - \boldsymbol{x}_A|$, and

$$\mathcal{A}(\theta) \coloneqq a_A^2(1-\epsilon_A^2\sin^2(\theta-\varphi_A)) + a_B^2(1-\epsilon_B^2\sin^2(\theta-\varphi_B))$$

and we evaluate final integral over θ numerically in *Mathematica* using the DOUBLEEXPONENTIAL method and a working precision and accuracy of 20.

B. Spherical spacetime

We will consider Gaussian detectors on the $(2+1)$-dimensional surface of the sphere. Without loss of generality the first detector, A, can be centered at the north pole. The center of the position of the second detector, B, is encoded through an arbitrary polar rotation θ and an azimuthal rotation φ relative to the north pole. To consider elliptical (or squeezed) detectors we introduce an additional parameter, γ, that describes the rotation of a profile about its semimajor axis. To study the response of the detectors we will need to calculate the spherical harmonics coefficients $f^D_{\ell m}$ and how they transform under an arbitrary rotation on the surface of the sphere.

A spherical analog of a Gaussian profile is the Fisher-Bingham five-parameter (FB5) distribution [41], given by

$$f(\hat{\boldsymbol{x}};\kappa,\hat{\boldsymbol{\mu}},\beta,\boldsymbol{A}) = \frac{1}{C(\kappa,\beta)}e^{\kappa\hat{\boldsymbol{\mu}}^T\hat{\boldsymbol{x}}+\hat{\boldsymbol{x}}^T\beta\boldsymbol{A}\hat{\boldsymbol{x}}}, \tag{63}$$

where

$$C(\kappa,\beta) = 2\pi\sum_{r=0}^{\infty}\frac{\Gamma(r+1/2)}{\Gamma(r+1)}\beta^{2r}(\kappa/2)^{-2r-1/2}I_{2r+1/2}(\kappa) \tag{64}$$

is the normalization constant $C(\kappa,\beta)$ and where $I_r(x)$ is the modified Bessel function of the first kind of order r. Moreover, $\boldsymbol{A}$ is a 3×3 symmetric matrix defined as

$$\boldsymbol{A} = (\hat{\boldsymbol{\eta}}_1\hat{\boldsymbol{\eta}}_1^T - \hat{\boldsymbol{\eta}}_2\hat{\boldsymbol{\eta}}_2^T), \tag{65}$$

where the unit vectors $\hat{\boldsymbol{\mu}}, \hat{\boldsymbol{\eta}_1}, \hat{\boldsymbol{\eta}_2}$ respectively correspond to the mean center, semimajor and semiminor axes of the FB5 distribution. The parameter $\kappa \geq 0$ quantifies the spatial concentration around the center $\hat{\boldsymbol{\mu}}$ and the parameter $\beta \leq \frac{\kappa}{2}$ quantifies the ellipticity of the distribution. The higher the values of κ and β are, the more concentrated and elliptical the FB5 distribution.

The rotation group SO(3) is the continuous group of all rotations around an origin in three-dimensional Euclidean space that preserve the inner product in $\mathbb{R}^3$ under composition. Any arbitrary rotation $R(\alpha,\beta,\gamma)$ (like that on the surface of a sphere) can be characterized by the Euler angles (α,β,γ) in the "zyz" convention: rotate first by an angle γ around the z axis, then rotate by an angle β around the y axis, and finally rotate by an angle α around the z axis, yielding

$$R(\alpha,\beta,\gamma) = e^{-\mathrm{i}\alpha L_z}e^{-\mathrm{i}\beta L_y}e^{-\mathrm{i}\gamma L_z}, \tag{66}$$

where L_i is the rotation generator in the ith direction. These satisfy the commutation relation

$$[L_i, L_j] = \mathrm{i}\sum_{k=1}^{3}\epsilon_{ijk}L_k \quad \forall\ i,j \in \{1,2,3\}. \tag{67}$$

The matrix elements of the rotation operator R in the $|l,m\rangle$ basis are given by the Wigner-D matrix

$$\langle \ell, m|R(\alpha,\beta,\gamma)|\ell', m'\rangle = \delta_{\ell\ell'}D^{\ell}_{mm'}(\alpha,\beta,\gamma) \tag{68}$$

and using the fact that $|\ell, m\rangle$ are eigenstates of the $\hat{L}_z$ operator we can write

$$\begin{aligned} D^{\ell}_{mm'}(\alpha,\beta,\gamma) &= \langle \ell, m|R(\alpha,\beta,\gamma)|\ell, m'\rangle \\ &= \langle \ell, m|e^{-\mathrm{i}\alpha L_z}e^{-\mathrm{i}\beta L_y}e^{-\mathrm{i}\gamma L_z}|\ell, m'\rangle \\ &= e^{-\mathrm{i}m\alpha}\langle \ell, m|e^{-\mathrm{i}\beta L_y}|\ell, m'\rangle e^{-\mathrm{i}m'\gamma} \\ &= e^{-\mathrm{i}m\alpha}d^{\ell}_{mm'}(\beta)e^{-\mathrm{i}m'\gamma}, \end{aligned} \tag{69}$$

where $d^{\ell}_{mm'}$ are the Wigner-d matrix elements [42]. The Wigner-d matrix elements allow us to transform the spherical harmonics coefficients $f^R_{\ell m}$ under a Euler rotation since

$$\begin{aligned} f^R_{\ell m} &= \langle \theta,\varphi|fR(\alpha,\beta,\gamma)|\ell, m\rangle \\ &= \sum_{\ell',m'}\langle \theta,\varphi|f|\ell', m'\rangle\langle \ell', m'|R(\alpha,\beta,\gamma)|\ell, m\rangle \\ &= \sum_{\ell',m'}\langle \theta,\varphi|f|\ell', m'\rangle\delta_{\ell\ell'}D^{\ell}_{m'm}(\alpha,\beta,\gamma) \\ &= \sum_{m'=-\ell}^{\ell}D^{\ell}_{m'm}(\alpha,\beta,\gamma)f_{\ell m'}. \end{aligned} \tag{70}$$

To derive these coefficients for an arbitrary FB5 distribution we follow the approach presented in [41], where we begin with an FB5 distribution centered at the north pole with the mean, semimajor and semiminor axes aligned as follows:

$$\hat{\boldsymbol{\mu}}^0 = [0\ \ 0\ \ 1]^T \quad \hat{\boldsymbol{\eta}}_1^0 = [1\ \ 0\ \ 0]^T \quad \hat{\boldsymbol{\eta}}_2^0 = [0\ \ 1\ \ 0]^T, \tag{71}$$

respectively. We will refer to this as the standard FB distribution $g(\hat{x};\kappa,\beta)$, with the general FB5 distribution (63) related to the standard one via

$$f(\hat{\boldsymbol{x}};\kappa,\beta,\hat{\boldsymbol{\mu}},\boldsymbol{A}) = R(\alpha,\beta,\gamma)g(\hat{x};\kappa,\beta). \tag{72}$$

This allows us to calculate the spherical harmonics coefficients $g_{\ell m}$ for the standard FB distribution and automatically obtain the spherical harmonics $f_{\ell m}$ for the general FB5 distribution through the transformation

$$f_{\ell,m} = \sum_{m'=-\ell}^{\ell}D^{\ell}_{m',m}(\alpha,\beta,\gamma)g_{\ell,m'}, \tag{73}$$

where $D^{\ell}_{m,m'}$ is the Wigner-d function of degree ℓ and $\{\alpha,\beta,\gamma\}$ are the Euler angles. Under these assumptions the standard FB distribution is given by

$$g(\hat{x};\kappa,\beta) = \frac{1}{C(\kappa,\beta)}e^{\kappa\cos\theta+\beta\sin^2\theta\cos 2\varphi}. \tag{74}$$

Consider first that detector A is unsqueezed ($\beta = 0$). Its probability distribution function g is then

$$g = \frac{\sqrt{\kappa}e^{\kappa\cos\theta}}{(2\pi)^{3/2}I_{1/2}(\kappa)} \tag{75}$$

using (64). We can derive an analytic expression for the spherical harmonics coefficients $g_{\ell m} = \langle g(\kappa,\beta,\theta), Y^m_\ell\rangle$

$$g_{\ell m} = \delta_{m,0}\sqrt{\frac{2\ell+1}{4\pi}}\frac{I_{\ell+1/2}(\kappa)}{I_{1/2}(\kappa)} \equiv \delta_{m,0}g_\ell \tag{76}$$

as shown in Appendix B.

If the detector is squeezed ($\beta \neq 0$) then these coefficients become

$$g_{\ell m} = 2\pi \frac{N_{\ell m}}{C(\kappa,\beta)} \int_{-1}^{1} e^{\kappa z} P_{\ell}^{m}(z) I_{m/2}(\beta(1-z^2)) dz \quad (77)$$

also shown in Appendix B, where $P_{\ell}^{m}(z)$ is an associated Legendre function. Note that the integral above is 0 whenever m is odd. The coefficients in (77) can be evaluated numerically for a given κ and β.

We shall place detector A at the north pole so that it is described by the standard FB distribution whose spherical harmonics coefficients $g_{\ell m}$ are given by (76) if unsqueezed and by (77) if squeezed. The second detector, B, is placed anywhere on the sphere via a Euler rotation, and its spherical harmonics coefficients are given by (73). The integrals are evaluated using the same method DOUBLEEXPONENTIAL as discussed at the end of the last subsection.

With this established, in Appendix B we show that the local coupling term for each detector can be simplified to

$$f_D = \exp\left[-\sum_{\ell=0}^{\infty}\sum_{m=-\ell}^{\ell} \frac{\lambda_D^2 \eta_D^2}{2\ell+1} |g_{\ell m}^{D}|^2\right]. \quad (78)$$

This is to be expected since the spacetime has constant spatial curvature everywhere, so we would not expect the detector localization to depend on where the detector coupled to the field. Furthermore, the smeared field commutator becomes

$$\Theta = i\lambda_A\lambda_B\eta_A\eta_B \sum_{\ell,m} \frac{1}{2(\ell+1/2)} \left[g_{\ell,m}^{A^*} \left(\sum_{m_1=-\ell}^{\ell} D_{m,m_1}^{\ell}(\alpha_B,\beta_B,\gamma_B) g_{\ell,m_1}^{B} \right) e^{i(\ell+1/2)(T_B-T_A)} - g_{\ell,m}^{A} \left(\sum_{m_1=-\ell}^{\ell} D_{m,m_1}^{\ell}(\alpha_B,\beta_B,\gamma_B) g_{\ell,m_1}^{B} \right)^{*} e^{-i(\ell+1/2)(T_B-T_A)} \right] \quad (79)$$

after substituting (73) into (54). In Appendix D we show that if both detectors are regular and the second detector is centered at an angle $\alpha = \theta$, then Θ can be simplified to

$$\Theta = i\lambda_A\lambda_B\eta_A\eta_B \sum_{\ell=0}^{\infty} \frac{1}{2\ell+1} [f_{\ell}^{A*} f_{\ell}^{B} P_{\ell}[\cos(\theta)] e^{i(\ell+1/2)(T_B-T_A)} - f_{\ell}^{A} f_{\ell}^{B*} P_{\ell}[\cos(\theta)] e^{-i(\ell+1/2)(T_B-T_A)}]. \quad (80)$$

IV. SINGLE DETECTOR RESULTS

We consider first the response of a single detector to a bandlimited field in both the Minkowski and spherical spacetimes. Note that a bandlimit is expressed as a cutoff Λ in momentum in flat spacetime, whereas it is expressed as a maximum value of ℓ (denoted as $\ell_{\max}$) in the spherical spacetime. In the spherical case we are unable to numerically sum over all values of ℓ, and so will always have to impose a cutoff at some maximal value.

A. Flat spacetime

The transition probability of a single UDW detector with a spatial profile given by Eq. (60) depends on three parameters: its size, a, its eccentricity, ϵ, and the bandlimit of the scalar field, Λ.

In Fig. 2, we plot the transition probability of a single UDW detector as a function of its size and eccentricity that couples to a field with no bandlimit ($\Lambda \to \infty$). We find that the transition probability of the detector increases as the overall size of the detector decreases for a given eccentricity, approaching a value of 0.5 in the pointlike limit. This is commensurate with previous results on bandlimited detectors [12], where it was shown that for a detector with an unsqueezed Gaussian spatial profile, smaller detectors have higher transition probabilities due to an increased

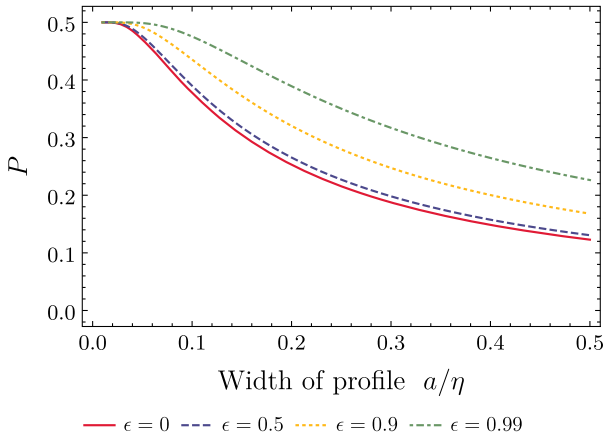

FIG. 2. The transition probability P of a single detector in flat spacetime that interacts with a scalar field with no bandlimit as a function of its size for various values of the eccentricity. The transition probability increases for decreasing detector size and increasing eccentricity. The dimensionless coupling constant is $\lambda\eta^{1/2} = 1$.

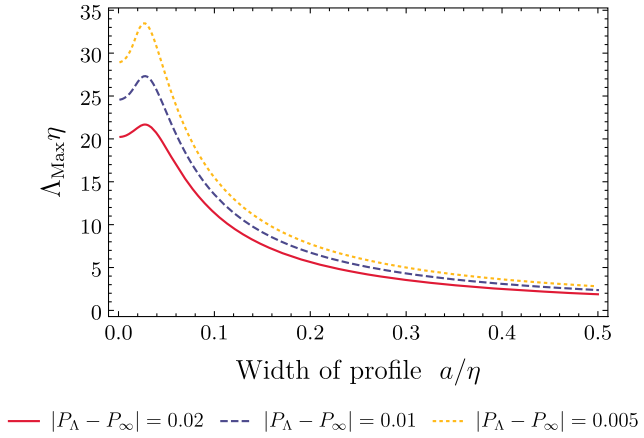

FIG. 3. The value of the maximum bandlimit Λ_{max} such that the difference between the transition probability in the bandlimtied field and the nonbandlimited field is equal to a specified (arbitrary) tolerance as a function of the size of the unsqueezed ($\epsilon = 0$) spatial profile in flat spacetime. The dimensionless coupling constant is $\lambda\eta^{1/2} = 1$.

sensitivity to high momentum field modes. We see that this behavior holds for squeezed detectors as well; detectors with a smaller overall size have a higher transition probability.

Conversely, for a given size, as the eccentricity increases, the transition probability also increases. We can understand this by noting that squeezing reduces the length scale of the profile in one direction, say the x direction. This will increase the sensitivity of the detector to field modes with a large momentum in the x direction, yielding a larger transition probability.

In order to explore the effect of detector squeezing on bandlimit detection, for a baseline comparison we first consider the case of an unsqueezed detector. In Fig. 3, we plot the value of the bandlimit Λ_{Max} for which the transition probability of an unsqueezed detector is within a chosen tolerance away from the corresponding nonbandlimited value ($\Lambda \to \infty$) as a function of detector size. We choose this value as a measure of bandlimit detection for two reasons. First, it provides a precise definition of when the bandlimited transition probability is "close" to its asymptotic value. Second, this value provides an operational notion of bandlimit detection. In an experimental setup, one can only distinguish between two measures to within some tolerance. Hence given a detector size and tolerance, there is a maximum value of field bandlimit that can be distinguished from the case with no bandlimit.

We find that, regardless of the chosen tolerance, small detectors are able to detect a higher bandlimit than larger detectors. However, once the detector's size is smaller than a (tolerance dependent) critical size, we find that within this regime larger detectors are able to detect larger bandlimit than smaller detectors. These results match what was presented for $(3+1)$-dimensional Minkowski space [12], suggesting dimensional independence.

In Fig. 4, we explore the impact of squeezing on bandlimit detection, and find that squeezing does not necessarily increase sensitivity to a bandlimit. Instead, we find the effect of squeezing depends on the overall size of the detector. If the detector is larger than the optimal size found in Fig. 3, then increasing the squeezing increases its sensitivity to the bandlimit, whereas if the detector is near or smaller than the optimal size, increased squeezing decreases its sensitivity to the bandlimit. Since squeezing reduces the length scale of the detector along one direction, this further suggests there is an overall optimal detector scale for bandlimit detection.

B. Spherical spacetime

Turning to the spherical case, in Fig. 5 we analyze the transition probability of a single detector as a function of its

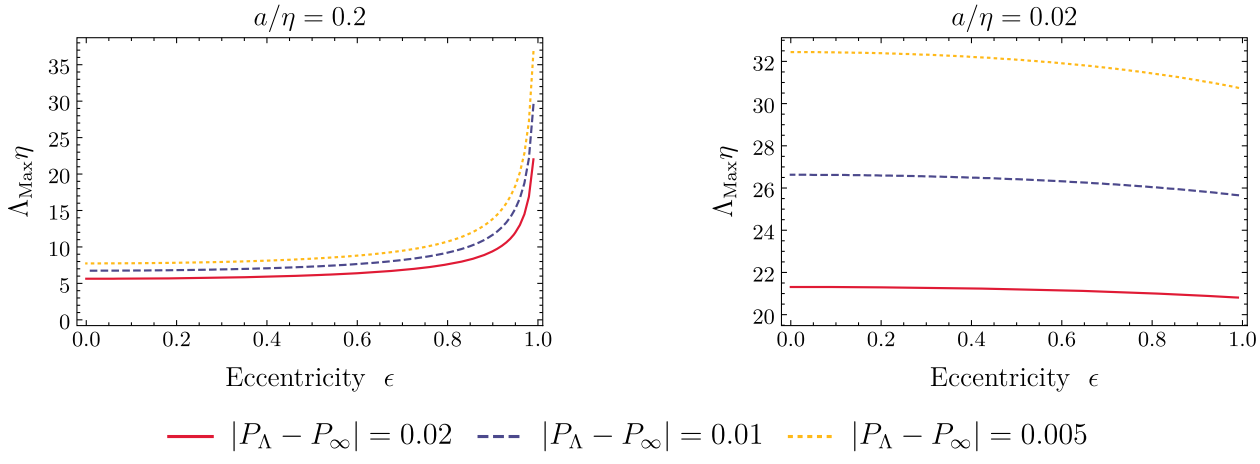

FIG. 4. The value in flat spacetime of the maximum bandlimit Λ_{max} such that the difference between the transition probability in the bandlimited field and the nonbandlimited field is equal to a specified (arbitrary) tolerance as a function of the eccentricity of the spatial profile for a detector size of (left) $a_A = 0.2\eta$ and (right) $a_A = 0.02\eta$. The dimensionless coupling constant is $\lambda\eta^{1/2} = 1$.

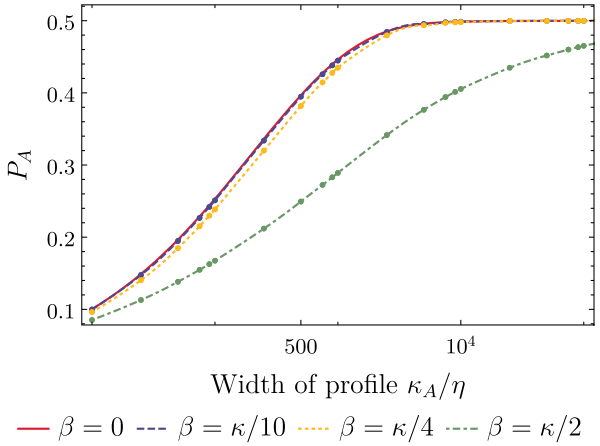

FIG. 5. The transition probability P of a single detector on a sphere that interacts with a scalar field with a bandlimit $\ell_{\max} = 100$ as a function of its size for various values of the squeezing parameter β. The transition probability increases for decreasing detector size and decreasing squeezing, the latter in contrast to the flat spacetime case. The dimensionless coupling constant is $\lambda\eta^{1/2} = 1$.

size κ for various values of the squeezing parameter β. The value of the bandlimit, $\ell_{\max}$, was set to 100, which is sufficient for the results to converge to a tolerance of 0.001, much smaller than the resolution of the figure. As in the flat spacetime setting, we see that the transition probability increases with decreasing detector size (increasing κ), approaching $1/2$ in the pointlike limit $\kappa \to \infty$. This is because smaller detectors have larger spherical harmonics coefficients, and so end up coupling to more field modes, analogous to the Fourier transform of the Gaussian shape in flat space. In addition, we see that contrary to flat space, squeezing decreases the response of a detector.

It is important to note that squeezing is implemented differently in the FB5 distribution [Eq. (74)] than in a two-dimensional Gaussian distribution [Eq. (57)]. While in both cases, increasing the squeezing parameter decreases the length of the semiminor axis and increases the length of the semimajor axis, the two distributions renormalize the function differently. The former case reduces the overall height of the distribution while the latter increases the overall height of the distribution. The mathematical consequence of this is that cross sections of the squeezed FB5 distribution are no longer Gaussians, whereas cross sections of the squeezed two-dimensional Gaussian distribution remain Gaussians. Functionally, this means that when a detector on a sphere is squeezed, it is more sensitive to field modes with higher momentum perpendicular to the direction of squeezing, but couple to them less strongly overall as compared to an unsqueezed detector.

To formalize the notion of optimal detection of a bandlimit we analyze the absolute difference between the transition probability of a bandlimited detector with one that is not bandlimited. In the absence of closed form expressions of the series sums that define the response of the detector, we take an $\ell_{\max}$ of 350 to be the value at which we truncate the series and call that "infinity." This value was chosen since the results converge up to machine precision. This $|P_{A,\infty} - P_{A,\ell_{\max}}|$ value will be the criterion for optimal bandlimit detection. The higher this absolute difference, the more sensitive a detector is (in some configuration) to the value of the bandlimit should it exist. Moreover, this absolute difference or tolerance criterion can be understood in an operational sense. That is, if we can resolve the transition probabilities of the detectors in an experimental setup up to an accuracy or a tolerance lower than the absolute difference between the nonbandlimited and the bandlimited response, then the bandlimit is detectable.

In Fig. 6, we plot the absolute difference between the nonbandlimited and bandlimited response as a function of the detector size for several values of $\ell_{\max}$. For clarity, we have made the plot of the tolerance continuous though the $\ell_{\max}$ bandlimit is discrete. In Fig. 6, we see that regardless of the chosen tolerance, for any bandlimit, there is a size where the detectors are optimally sensitive to the presence of a bandlimit. In other words bandlimit detection is optimal for small but not pointlike detectors exactly like detectors in flat spacetime.

The interplay between the size of the detector and optimal bandlimit detection can be understood as follows. First, the existence of an optimal size for bandlimit detection can be explained by recasting the detection criterion differently. Ultimately, what we are investigating is the contribution of each field mode to the response of the detector. In light of that, the absolute difference would be dictated by how the length scale of the detector determines its coupling to the field. Larger detectors couple weakly so they are only sensitive to a very small bandlimit. On the other hand, pointlike detectors couple to every field mode,

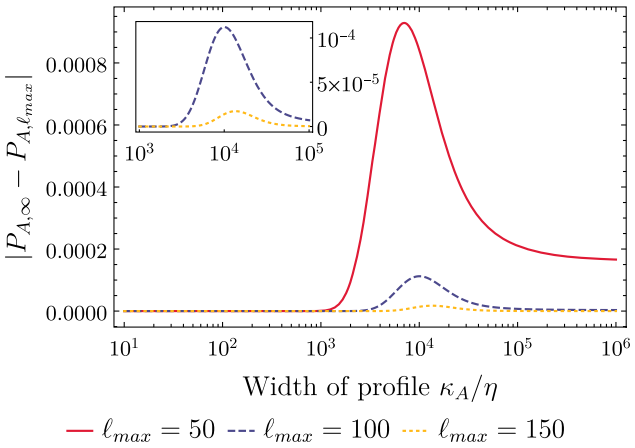

FIG. 6. The value of the absolute difference bandlimit detection criterion of a single regular detector ($\beta = 0$) on the sphere as a function of the detector size for several values of the bandlimit $\ell_{\max}$. The dimensionless coupling constant is $\lambda\eta^{1/2} = 1$.

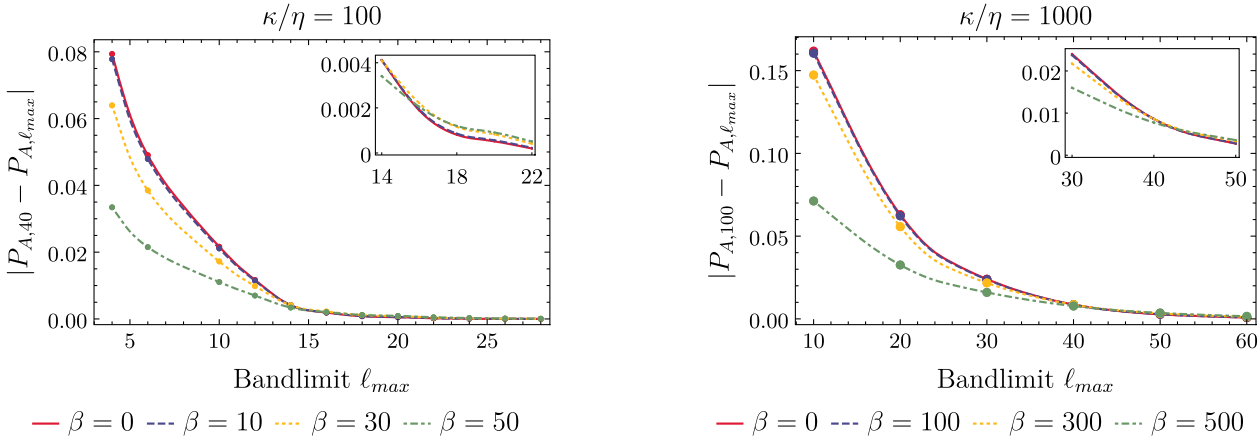

FIG. 7. The absolute difference bandlimit detection criterion for squeezed detectors as a function of the cutoff ℓ_{max} for several values of the squeezing parameter. Note that ℓ_{max} is a discrete parameter, so the interpolation done between the data points in the figures is done for purely illustrative purposes. Left: The detector size is set to $\kappa = 100\eta$. Right: It is set to $\kappa = 1000\eta$. The dimensionless coupling constant is $\lambda\eta^{1/2} = 1$.

as demonstrated by Eq. (53) in the limit as $\kappa \to \infty$. The optimal length scale is a balance between both effects: we want a sensitive detector that can couple to many of the field modes but not to be so small (near pointlike) that it is too sensitive, making its response saturate to $1/2$. In other words, we do not want it to become a maximally mixed state where we cannot resolve the impact of the cutoff on its response.

Finally, we consider the impact of squeezing on bandlimit detection. In Fig. 7 (left), we pick a large nonoptimal size of $\kappa = 100\eta$ and analyze the bandlimit detection criterion as a function of the cutoff $\ell_{\max}$ for several values of the squeezing parameter β. Because of numerical considerations, the values of ℓ_∞ chosen were based on the values calculated where the results have converged in Fig. 6 as opposed to some arbitrary tolerance. Contrary to the behavior in flat space shown in Fig. 4, squeezing decreases the sensitivity to the bandlimit. However, this is only true up to a certain value of $\ell_{\max}$, where we observe a nominal increase in bandlimit detection. This pattern holds for the smaller $k = 1000\eta$ detector [as shown in Fig. 7 (right)], which is closer to the optimal size as discussed for Fig. 6. This implies that the optimality of squeezing in this context is dependent on the value of the bandlimit itself. This is in notable contrast to flat space, where the optimality (or lack thereof) of squeezing depended primarily on the size of the detector. Ultimately, optimal bandlimit detection is not just set by the best scale for probing field fluctuations, but also by the geometry of the background spacetime (encoded in the fluctuations) and the geometry of the detectors.

V. RESULTS FOR TWO DETECTORS

A. Signaling and the structure of the smeared field commutator

In the two detector setup, if both detectors are casually connected, the second detector will interact with an evolved state of the field locally due to the interaction of the first detector with the field. The response of the second detector will then depend (in part) on the field mediated signaling from the first detector. To that end, let us consider the two point Wightman distribution W for a scalar field $\hat{\phi}$. The Wightman distribution can be split into a real and an imaginary part as

$$W(\mathrm{x},\mathrm{x}') := \frac{1}{2}(W^+(\mathrm{x},\mathrm{x}') + W^-(\mathrm{x},\mathrm{x}')), \tag{81}$$

where the real and imaginary contributions are defined as

$$\begin{aligned} W^+(\mathrm{x},\mathrm{x}') &= \langle 0|\{\hat{\phi}(\mathrm{x}),\hat{\phi}(\mathrm{x}')\}|0\rangle \\ W^-(\mathrm{x},\mathrm{x}') &= \langle 0|[\hat{\phi}(\mathrm{x}),\hat{\phi}(\mathrm{x}')]|0\rangle, \end{aligned} \tag{82}$$

and so W^+ and W^- are the vacuum expectation values of the field anticommutator and commutator respectively. The operators ω and Θ defined in Eq. (20) are smeared versions of W^+ and W^- due to the smearing of the detectors over a compact region of spacetime. Studying the structure of the field commutator is of utmost importance when considering two detectors in causal contact, since it encodes causal signaling through the field between the spacetime regions where the detectors are.

In particular, the strong Huygen's principle states that the solutions of a hyperbolic second-order linear partial differential equation have support only along the null direction. In general, however, this does not hold for a massless scalar field on a curved background and only holds in $n+1$ flat spacetime for odd dimensional $n \geq 3$ [43]. To illustrate this, consider the Green's function for the massless scalar field in $2+1$ Minkowski spacetime,

$$G(\boldsymbol{x},t,\boldsymbol{x}',t') = \frac{\mathrm{i}}{2\pi}\frac{\mathrm{sgn}(t'-t)H((t-t')^2-|\boldsymbol{x}-\boldsymbol{x}'|^2)}{\sqrt{(t-t')^2-|\boldsymbol{x}-\boldsymbol{x}'|^2}}, \tag{83}$$

where $H(x)$ is the Heaviside function. It is important to note that due to the $\mathrm{sgn}(t'-t)/\sqrt{(t-t')^2-|\boldsymbol{x}-\boldsymbol{x}'|^2}$ prefactor, part of the signal travels along timelike geodesics inside the light cone. On the spherical spacetime, for two events separated by a time T at two arbitrary positions, the Green's function can be expanded in terms of spherical harmonics modes as [40]

$$G=\frac{1}{4\pi}e^{-\mathrm{i}T/2}\sum_{\ell=0}^{\infty}e^{-\mathrm{i}\ell T}P_{\ell}(\cos(\alpha)), \tag{84}$$

where T is the difference in time between two events and α is the total angle between (θ,φ) and (θ',φ'). Then using the generating function of the Legendre polynomials, $\sum_{n=0}^{\infty}P_n(x)z^n=(1-2xz+z^2)^{-\frac{1}{2}}$ for $-1<x<1$ and $|z|<1$, we can write G as

$$G(\theta,\varphi,\theta',\varphi')=\frac{1}{4\sqrt{2}\pi}[\cos(T-\mathrm{i}\epsilon)-\cos\theta\cos\theta' -\sin\theta\sin\theta'\cos(\varphi-\varphi')^{-\frac{1}{2}}], \tag{85}$$

where $\mathrm{i}\varepsilon$ is a regularization term that is taken to 0 at the end of any calculation. Two salient features are implicit in (85). One is that G has support inside the entirety of the light cone; the other is that it diverges along the null $\theta=T$ geodesics. The former is a general feature of Green's functions of scalar fields on curved spacetimes.

The dependence of any field-mediated signaling in the response of the second detector is encoded in the smeared field commutator. In the absence of a bandlimit, it is expected that the smeared field commutator becomes the imaginary part of the Green's function $\Theta\sim\mathrm{Im}[G]$. To see this, consider the pointlike limit of both detectors $\lim_{\kappa_D\to\infty}f_{\ell}^{D}=\sqrt{\frac{2\ell+1}{4\pi}}$. Inserting this into (80) yields

$$\Theta=\frac{i\lambda_A\lambda_B\eta_A\eta_B}{4\pi}\sum_{\ell=0}^{\infty}P_{\ell}(\cos(\theta))\sin((\ell+1/2)T)\sim\mathrm{Im}[G], \tag{86}$$

where G is given by (84).

Now, let us try to relate Θ to the Green's function G to understand the role of the detector smearing on the production and detection of the signal through the scalar field. We consider the case of two symmetric detectors in the absence of a bandlimit so that the smeared field commutator is given by (80). Structurally, this is nothing other than multiplying each mode of the Green's function by the product of the modes $f_{\ell}^{A}f_{\ell}^{B}$ (since the mode coefficients are real). The convolution of two functions f, g defined on S^2, where one of them is azimuthally symmetric, is defined as [44]

$$(f\circledast g)_{\ell m}=\sqrt{\frac{4\pi}{2\ell+1}}f_{\ell m}g^{*}_{\ell 0} \tag{87}$$

in the harmonic basis. Equation (84) is a spherical convolution between the two functions $(f^Af^B)\circledast G$ defined on S^2, where f^Af^B is the product of the Gaussian smearing functions of the detectors A and B and G is the Green's function. This implies that if the field is bandlimited and coupled to smeared detectors, signaling from the first detector to the second is encoded in a bandlimited convolution of the product of the detector sizes with the Green's function G. This modulates the individual modes of G and controls the strength of the signal inside the light cone. For small first detectors, most of the contribution of the signal will be along the light cone and for large first detectors, the signal trails inside the light cone.

With all of this established, we now analyze the structure of the smeared commutator. First, we note that it is symmetric under the exchange of detector sizes. This is due to the fact that the localization of the detectors does not depend on their positions in a stationary spacetime [30]. In addition, if we switch the second detector "off time," i.e. $\theta\neq T$, so that the peak switching time of the second detector is not coordinated with the peak of the signal from the first detector, the modes of the smeared commutator add up to 0 and the $\cos(2\Theta)$ contribution to the second detector's response vanishes. In other words, if the second detector is switched on too early or too late, thereby "missing" the signal from the first detector, it effectively couples to the vacuum and microcausality is maintained.

Finally, the smeared commutator is reflection symmetric in time about $t=\pi$, i.e. $\Theta(t,\theta,\varphi)=\Theta(t-\pi,\theta,\varphi)$. This property is inherited entirely from the Green's function (85). This would indicate that any signal from detector A and the response of detector B would also have to follow this reflection symmetry in time. We can make all these features concrete by treating the second detector as a proxy to the signal from the first. In Fig. 8, we plot the transition probability of a regular detector B of size $\kappa=100$ as a function of the polar angle θ where it is centered and $T:=T_B-T_A$, or in other words where and when it coupled to the field relative to the first detector. The first detector also has a size of $\kappa=100$ and was coupled to the field at $T_A=0$. First, we see that the signal is concentrated along the light cone ($\theta=T$) from the north to the south pole because of the higher excitation probability of detector B. In addition, if the second detector misses the signal from the first detector when switched off time, then its excitation probability is that of a detector that coupled to the vacuum as discussed earlier, shown as the dark blue shading in the figure. Finally, we can see the time symmetry of the signal manifest in the response of the second detector through the reflection along the line $T=\pi$ in the figure.

B. Response of two detectors and bandlimit detection on $R\times S^2$

We now turn our attention to bandlimit detection with two detectors. Can we exploit the field-mediated signaling

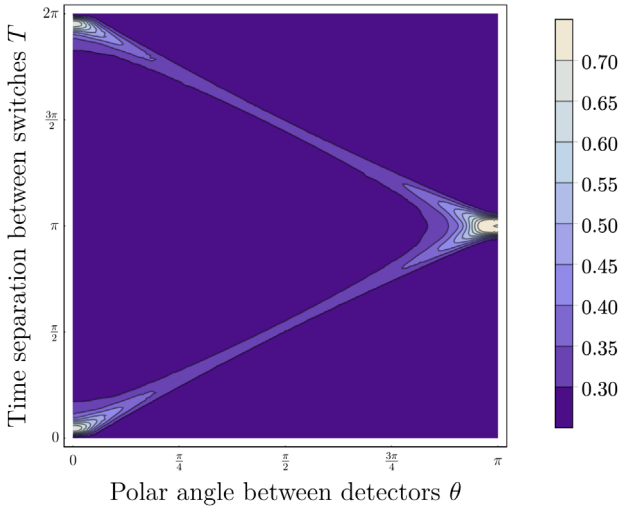

FIG. 8. The response of the second detector on the spherical spacetime as a function of spacetime separation between coupling the first and second detectors. Both detectors are equally sized with size $\kappa = 100\eta$. The dimensionless coupling constant is $\lambda\eta^{1/2} = 1$.

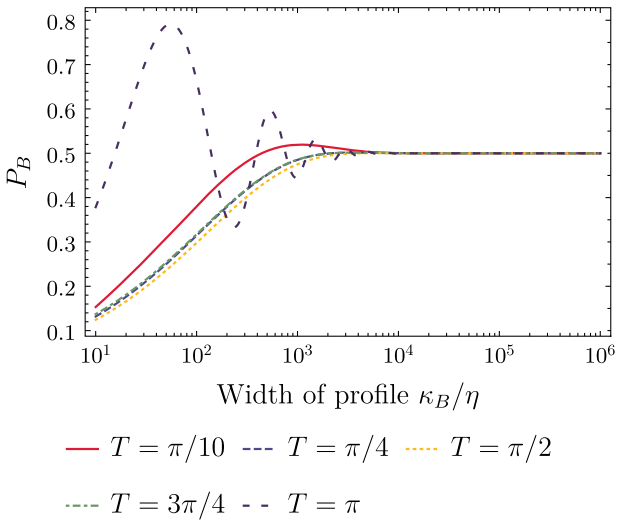

FIG. 9. The response of the second detector on the spherical spacetime switched on time as a function of the size of the second detector for various spatial separations between the detectors. The first detector is assumed to be pointlike and the bandlimit is set to $\ell_{\max} = 200$. The dimensionless coupling constant is $\lambda\eta^{1/2} = 1$.

to find an optimal length scale or an optimal spacetime separation on the spherical spacetime for the detection of the bandlimit?

In flat space we find that, although the smeared field commutator Θ depends heavily on the bandlimit, the transition probability of the second detector does not. Consequently, we do not get a large gain in bandlimit detection by employing two detectors. However, when the detectors are on a sphere the signal from detector A does not dissipate (unlike in flat space) and instead becomes focused at the antipodal region. By placing the second detector at that location, we can maximize the effect of the commutator, and hence the sensitivity to the bandlimit.

Given the liberty to localize the second detector anywhere on the spherical spacetime, we study the response of the second detector placed at several distinct latitudes along an arbitrary line of longitude. We will only consider a pair of regular/unsqueezed detectors when analyzing bandlimit detection as per our discussion in Sec. IV. We begin by coordinating the switching time of the second detector with the peak of the signal; in other words we switch on the second detector on the $\theta = T$ part of the light cone. We will refer to this as switching "on time."

In Fig. 9 we depict the response of the second detector B as a function of its size, switched on time at several different values of T. Detector A is chosen such that it is pointlike and we will consider a bandlimit of $\ell_{\max} = 200$. As discussed in Sec. V A, the modes through which the signal propagates depend on the size of the first detector. Consequently, we consider the first detector to be pointlike so as to not impose an effective cutoff when probing the bandlimit via signaling. The response of the second detector is qualitatively similar to that of a single detector, as shown in the $\beta = 0$ curve of Fig. 5, for switches on time at $\theta = \frac{\pi}{4}, \frac{\pi}{2}$ and $\frac{3\pi}{4}$. We also observe that the response for detectors placed at $\frac{\pi}{4}$ and $\frac{3\pi}{4}$ is identical, as expected due to the symmetry of the spacetime. The slowest increase in response of the second detector is for the $\frac{\pi}{2}$ case.

The most interesting behavior in the response is for a switch at each pole ($\theta = \pi$). We see that it can be larger than $1/2$, oscillating as a function of the detector size. In the pointlike (large-κ) limit, the response converges to $1/2$. This is because the support of the smearing of detector B becomes too small to resolve the effects of curvature of the spacetime on the field; as expected, its response asymptotes to the pointlike response regardless of where and when it coupled to the field.

It is worth reiterating that since the spacetime is stationary with constant curvature then the spatial profiles of the detectors do not depend on their location in the spacetime. This implies that the differences in the behavior of the response of detector B can be attributed to the field mediated signaling. In particular, due to the compact and bounded nature of the spacetime, the various switches in Fig. 9 interact with the signal through the field as it spreads from detector A all the way down as it gets focused at the south pole.

The geometric notion of the field-mediated signal spreading and focusing manifests itself through the smeared field commutator and its modes. To this end, let us analyze the dependence of the smeared commutator on the individual ℓ modes. In Fig. 10 (left), we plot Θ as a function of κ_B for various values of ℓ modes of the smeared commutator Θ, denoted by Θ_ℓ, in increments of 20 when

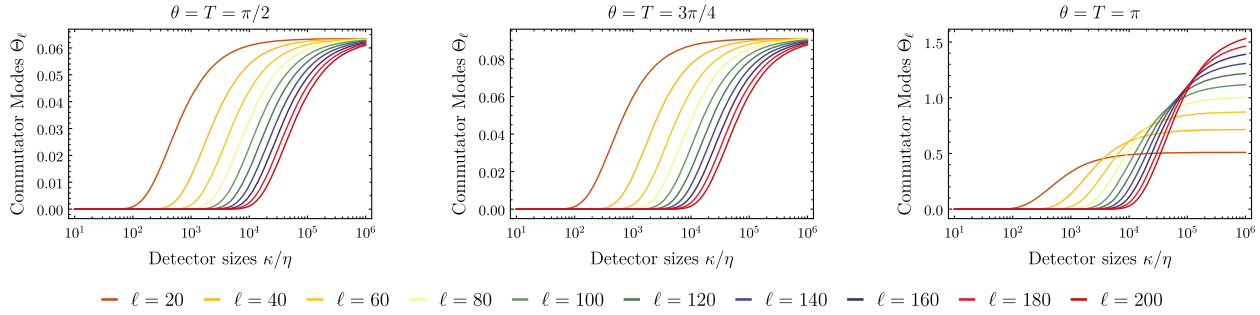

FIG. 10. The value of the commutator modes Θ_ℓ as a function of the size κ/η of both detectors at various spatial and switching time separations. Left: The second detector is switched on at $\theta = T = \pi/2$, Center: at $\theta = T = 3\pi/4$, Right: at $\theta = T = \pi$. The dimensionless coupling constant is $\lambda\eta^{1/2} = 1$.

the second detector is switched on time at $\pi/2$. This choice corresponds to a maximally spread signal. However, we also find that the pattern in Fig. 10 (left) holds as the on time switch increases to $3\pi/4$ (as the signal becomes more focused), as shown in Fig. 10 (center). We see that all the commutator modes Θ_ℓ asymptote to a value $\tilde{\Theta}(\theta)$ regardless of the ℓ mode in the pointlike limit $\kappa_B \to \infty$. Moreover, higher ℓ modes are suppressed at small κ_B, and only contribute to the smeared commutator Θ on length scales where the exponential suppression of the local coupling term is strong. Ultimately, the smeared commutator $[\Theta(\theta, T) = \sum_{\ell=0}^{\ell_{\max}} \Theta_\ell(\theta, T)]$ for all $\theta = T$ configurations where the signal is not entirely focused provides small corrections to the response of the second detector. Consequently, this provides us with a nominal improvement to bandlimit detection at best.

The situation as the second detector is switched on time at π (at the south pole) is different. As we can see in Fig. 10 (right), the individual contributions to the commutator are 2 orders of magnitude larger on average than those at maximal spread, shown in Fig. 10 (left). Moreover, the maximum value a mode has as a function of size increases as ℓ increases. So the commutator increases rapidly as a function of decreasing size (increasing κ_B), causing the signaling part of the response $[\cos(2\Theta)]$ to oscillate more rapidly. While this accounts for the behavior of the transition probability of the second detector, the rate of increase in the value of the commutator as a function of decreasing size also depends on the value of the bandlimit $\ell_{\max}$. In Fig. 11 (left) we plot the response of the detector switched on time at $T = \pi$ against its size. We see for sufficiently small but not pointlike detectors that oscillations in the response become distinct for different bandlimits. This offset in frequency could provide a promising candidate for more optimal bandlimit detection, since the response for a given size becomes more dependent on the bandlimit over this intermediate range of detector sizes.

With all of this established, we now know the optimal location for B that maximizes the contribution of the signal to B's response. We now consider the optimal sizes of the detectors. In the previous subsection, we saw how the size of the first detector dictates the modes through which the signal propagates. Ideally, detector A should be as small as possible, so as to allow detector B full sensitivity to an

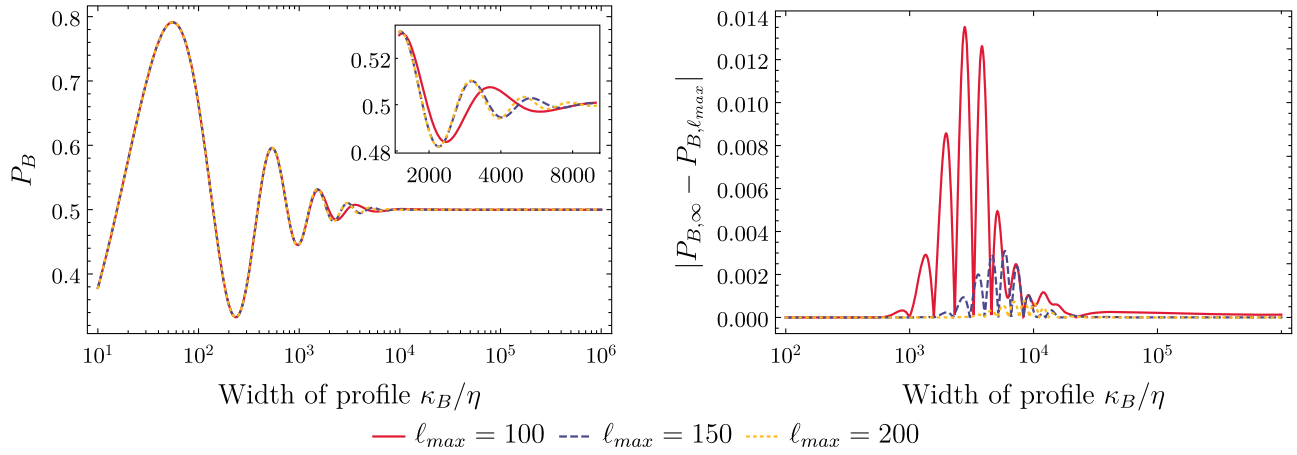

FIG. 11. Left: the transition probability P of a second regular detector switched on time at the pole as a function of its size for various values of the bandlimit $\ell_{\max}$. Right: the absolute difference bandlimit detection criterion for a regular second detector localized at the pole as a function of its size for several values of the bandlimit $\ell_{\max}$. For both plots, the dimensionless coupling constant is $\lambda\eta^{1/2} = 1$.

arbitrary value of the bandlimit. As such, we assume detector A to be pointlike.

Recall from Sec. IV that the large κ limit

$$\lim_{\kappa_A\to\infty} f_\ell^A = \sqrt{\frac{2\ell+1}{4\pi}}$$

is the pointlike limit, with the detector modes are given as above. The smeared commutator in the pointlike limit is

$$\lim_{\kappa_A\to\infty} \Theta = \sum_{\ell=0}^{\ell_{\max}} \frac{f_\ell^B P_\ell(\cos\theta)}{\sqrt{\pi(2\ell+1)}} \sin\left(\left(\ell+\frac{1}{2}\right)T\right). \tag{88}$$

In Fig. 11 (right), we plot for different $\ell_{\max}$ the bandlimit detection parameter for detector B as a function of its size κ_B when it is localized at the south pole and switched on time ($\theta = T = \pi$), with the first detector pointlike. We highlight several key features. First, the detection parameter is as much as a full order of magnitude larger than its single-detector counterpart, shown in Fig. 6. In addition, there is no longer a fixed optimal size for bandlimit detection: the range of optimal length scales now depends on the value of the bandlimit. Within this range, the bandlimit detection parameter oscillates. The origin of both effects is rooted in the reason as to why the response oscillates in the first place. As κ_B increases, Θ likewise increases, and so $\cos(2\Theta)$ can oscillate over several periods. This implies that the bandlimit detection criterion using a second detector can be recast as finding the length scale at which the rate of change of the sum of the ℓ modes of the commutator increases the fastest as a function of the detector size.

In flat spacetime the dominant effect on bandlimit detection is the local coupling of the detector as governed by its size [12]. With two detectors, the smeared commutator is much more sensitive to the bandlimit, but gets exponentially suppressed by the local detector coupling. On the spherical spacetime we have engineered a situation where the commutator grows rapidly as the bandlimit increases for all sizes such that the $\cos(2\Theta)$ signaling term rapidly oscillates, counteracting the exponential suppression from the local detector coupling term that happens before the pointlike limit of the detector is reached. In other words, we have engineered a situation where the sensitivity of the commutator to the bandlimit is manifest.

C. Squeezed detectors

To complete the exploration of the parameter space, we now allow both detectors to be in squeezed states. They can then be rotated relative to each other. We shall consider the effects of such rotations on the transition probability of the second detector.

We first identify four distinct detector configurations; taken together these allow for a robust exploration of the parameter space. Without loss of generality, we orient the coordinate system so that the semimajor axis of detector A is along the x axis in Minkowski space and at $\varphi = 0$ on a sphere. Placing the centroid of detector B at a fixed distance from that of A, its semimajor axis is then taken to be either parallel or perpendicular to that of detector A, resulting in the four configurations shown in the left column of Fig. 12. In case 1, the semimajor axis of B is always parallel to the semimajor axis of A. In case 2, the semimajor axis of B is always perpendicular to A. In case 3, the semimajor axis of B always points toward the center of A and in case 4, the semiminor axis of B always points toward the center of A. For the $R\times\mathbb{S}^2$ spacetime we set the orientation of B at the north pole and then parallel transport it to the coordinates (θ_B, φ_B) using Wigner-d functions.

1. Flat spacetime

Considering first the situation in flat space, shown in the center column of Fig. 12, we plot the transition probability of detector B as a function of its position. For convenience, we will define the position of B relative to A in terms of the vector $\boldsymbol{S} = (S, \varphi)$, with magnitude, S, describing the distance between the centers of the spatial profiles of the two detectors and angle, φ, relative to the semimajor axis of detector A. The angle that the semimajor axis of detector B makes with the vector $\boldsymbol{S}$ is determined by which of the four configurations is being considered.

We find that in all four cases, the field mediated signal from detector A leads to an increase in the transition probability of detector B as compared to the case when detector A does not switch. Since both detectors have a compact spatial extent, the signal from A will increase the transition probability of B for separations of their centroids that are greater than the time delay of their switching. However, the maximum increase occurs, for a given value of φ, when the separation between the detectors is slightly less than the time delay of their switching, i.e. when the center of the signal from A is slightly past the center of B at the time of switching. The specific effect of the signal depends on the choice of configuration.

In cases 1, 3, and 4, we find that the transition probability of the second detector depends significantly on the angle, φ, between the line connecting the centers of the two detectors and the semimajor axis of detector A, with the maximum occurring for $\varphi = \pi/2$ and $\varphi = 3\pi/2$. From the left column of Fig. 12, it can be seen that these angles correspond to the configuration where the vector S is coincident with the semiminor axis of A, indicating that the signal from A is strongest along this direction.

Additionally, we find dependence of the transition probably of B on the angle the semimajor axis of B makes with the vector $\boldsymbol{S}$, which is most straightforwardly demonstrated by comparing cases 3 and 4. In case 3, the semimajor axis of detector B lies along $\boldsymbol{S}$, while in case 4, the semimajor axis of B is perpendicular to $\boldsymbol{S}$. We find that

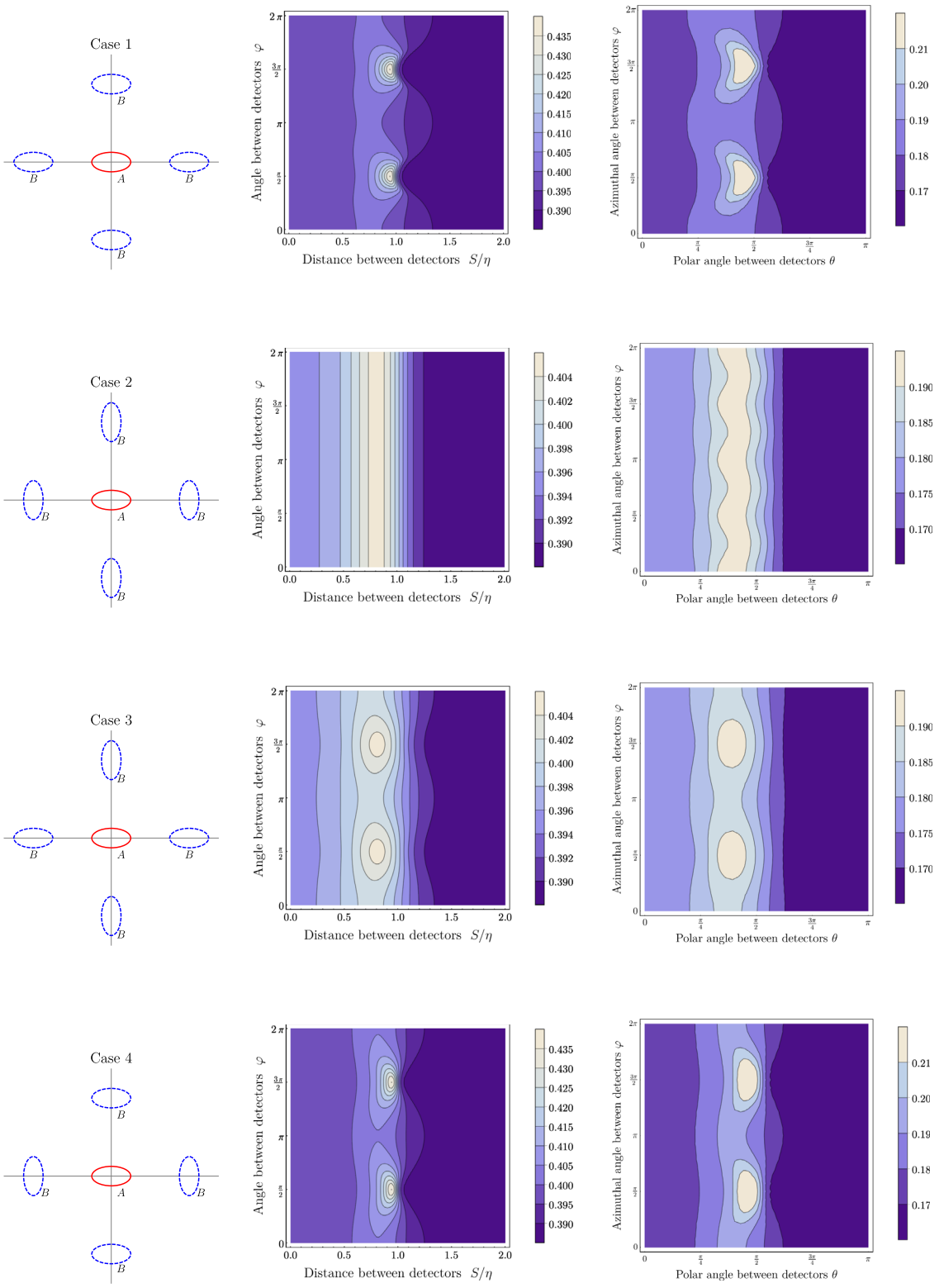

FIG. 12. Left: a schematic depicting the position of detector A and various positions of detector B for the four types of configurations considered, where each case is a new row. When the detectors are on the sphere, these figures are interpreted as top-down view of the north pole. Center: the transition probability of detector B in flat space as a function of the separation of the centers of the detectors, S, and the angle between detectors, φ. The time delay is $T = \eta$ and the detectors have a width of $a = 0.2\eta$ an eccentricity of $\epsilon = 0.99$. Right: the transition probability of detector B in spherical spacetime as a function of the polar θ and azimuthal φ separation between the centers of the detectors. The time delay is $T = \pi/2$ and the detectors have a size $\kappa = 100$ and a squeezing of $\beta = 50$.

when detector B is placed at the optimal distance from A, the transition probability of B is larger in case 4 than in case 3, which suggests that the detector is most sensitive to signals that propagate in a direction perpendicular to its semimajor axis.

In case 2, the orientation of B is fixed with its semimajor axis perpendicular to the semimajor axis of A, as shown in row two of the left column of Fig. 12. The effect of this configuration in flat space (row two of the center column of Fig. 12) removes any dependence of the angle φ from the transition probability of detector B; it only depends on the distance between the centers of the two detectors, S. This case most clearly demonstrates that the transition probably of B is greatest when the separation between the centers of the detectors is slightly less than the time delay between their switching. It also shows that the two orientation effects, the strength of the signal from detector A and the sensitivity of detector B, are of equal importance. By fixing the semimajor axis of B to remain perpendicular to the semimajor axis of A, it will be perpendicular, and hence the most sensitive, to the signal from A when the vector $\boldsymbol{S}$ is coincident with the semimajor axis of A ($\varphi = 0$ and $\varphi = \pi$). At these angles, the signal from A is the weakest. This fixed angle also ensures that when detector B is located where the signal from A is the strongest ($\varphi = \pi/2$ and $\varphi = 3\pi/2$) its semimajor axis will be coincident with the vector $\boldsymbol{S}$ and be the least sensitive to the signal from A. Since both cases (and all other values of φ) give the same transition probability for detector B, we can conclude that neither orientation effect is more important in increasing the transition probability of detector B.

We can interpret the relative strength of the signal and sensitivity of the detector to the relative length scale of the detector as follows. Recall that squeezing increases the sensitivity of the detector to field modes that have large momenta in the squeezing direction, so we expect detectors to be more sensitive to signals that propagate along the direction of their semiminor axis. Likewise we expect the signal sent by the squeezed detector A to contain more field modes with high momenta in the direction of squeezing, namely the semiminor axis.

2. Spherical spacetime

Next, we consider the case where the two detectors are on the surface of the sphere, illustrating the results in the right column of Fig. 12 for the four orientations illustrated in the left column of the same figure, where we now interpret the figures to be a top-down view of the north pole of the sphere. Detector A is located with its center at the north pole of the sphere with its semimajor axis aligned with $\varphi = 0$; therefore, the two angles describing the relative orientation of the two detectors, θ and φ, are the azimuthal and polar angle respectively.

Overall, we find a similar relationship between the transition probability of detector B to its relative position and orientation to detector A as we did in flat space. The transition probability of B is greatest when the distance between the centers of the detectors, θ, is slightly less than the time delay between their switching times, which can be seen most clearly in case 2.

Again, in cases 1, 3, and 4, we note that when the detector B is located at the optimal distance from A, the transition probably of B is maximized for $\varphi = \pi/2$ and $\varphi = 3\pi/2$. These orientations correspond to the case where the line connecting the centroids of the two detectors is coincident with the semiminor axis of A. Since the maximum occurs at this position, independent of the orientation of B, we conclude the field mediated signal from A is the strongest in this direction.

By comparing cases 3 and 4, we are able to isolate the dependence of the transition probability of B on its orientation relative to detector A. We find, analogous to the flat space case, that when B is located at the optimal value of θ, the transition probability is larger in case 4. In this case, B is oriented so its semimajor axis lies along a constant value of θ, i.e. it is perpendicular to the direction of propagation of the signal from A, which suggests that B is most sensitive to the signal that propagates in this direction.

Case 2 illustrates that unlike in flat space, orienting detector B so that its semimajor axis is perpendicular to the semimajor axis of detector A *before* it is parallel transported to the given value of (θ, φ) does not remove the φ dependence. This suggests that the effect of the anisotropy on the signal from A and the effect of orientation on the sensitivity of B do not cancel each other out the way they do in flat space, likely due the curvature of the sphere distorting the shape of detector B.

In both cases, we find that the signal from A that propagates in the direction perpendicular to its semimajor axis is the strongest and is weakest in the direction of propagation parallel to its semimajor axis. Similarly, detector B is most sensitive to the signal when it is oriented so that its semiminor axis is parallel to the direction of signal propagation and is the least sensitive to signals that with a direction of propagation parallel to its semimajor axis. We understand both of these effects as resulting from the effective bandlimit of the shape of the detector. These detectors are smaller in the direction of their semiminor axis, say the y axis, so are able to interact with field modes of higher frequency in that direction, here k_y. Therefore, detectors will be more easily excited by signals propagating in this direction, since more of the signal will interact with the detector, and detectors that signal through the field are able to access more modes in this direction, which will lead to stronger signals.

VI. CONCLUSIONS

We have exactly calculated the density matrix describing the state of two UDW detectors, each with a squeezed Gaussian smearing function, that each couple to a

conformal scalar field via Dirac-delta switching. We considered this on a $(2+1)$-dimensional spherical spacetime and on $2+1$ Minkowski spacetime for comparison. For both spacetimes we implemented a conventional bandlimit on the field by imposing a hard cutoff of the angular momentum modes in the former case and the linear momentum modes in the latter case.

For a single unsqueezed UDW detector, we found for both spacetimes that the results were analogous to those obtained previously in $3+1$ Minkowski space [12]. There is an optimal size detector for bandlimit detection—small, but not too small. We also found that in Minkowski space, when the smearing function is a squeezed Gaussian, and the overall size of the detector is larger than the optimal size, higher squeezing significantly increases sensitivity to the bandlimit. However if the detector is smaller than the optimal size, squeezing slightly decreases its sensitivity.

In considering two detectors, while a no-go theorem [33] prevents them from becoming entangled through this interaction, they can signal to each other. When the detectors are on a sphere, and the first detector, detector A, is located at the north pole, we found that the signal caused by A interacting with the field is reflection symmetric about $t=\pi$, that is the signal at (t,θ,φ) is the same at $(t-\pi,\theta,\varphi)$, and this property is inherited from the Green's function.

Since a sphere is compact, the signal from A does not dissipate and has a much more significant effect on the transition probability of the second detector B, particularly when it is located at the south pole. The specific effect depends heavily on the switching time and the size of the detector. Additionally, by tuning the switching time and size of the second detector appropriately, it can become significantly more sensitive to the bandlimit than can a single detector alone. This is in notable contrast to flat spacetime: since the signal can dissipate in Minkowski space, the transition probability of a second detector does not depend heavily on the signal from the first detector, and as a result cannot be used to significantly increase bandlimit detector capabilities.

Finally, we explored the effect of squeezing on the response of the second detector, and found that for both Minkowski and spherical spacetime, a Gaussian detector is most sensitive to a signal when it is orientated so that its semimajor axis is perpendicular to the direction of propagation. Similarly, the strongest signal from a Gaussian detector propagates in the direction perpendicular to its semimajor axis. Both effects are due to the detectors having the smallest length scale along their semiminor axis, which leads to field interactions accessing field modes with higher momenta in that direction. This optimization could be exploited to maximize communication between a pair of detectors, such as quantum collect calling [45], or to minimize signal jamming [46].

Our results can be naturally extended to AdS_3, which can be constructed as a conformal transformation of the sphere, and further extended to the BTZ black hole spacetime.

Overall, we exactly calculated the signaling between two detectors on a compact curved spacetime, and found, as a consequence of the compactness of a sphere, an order of magnitude improvement on local bandlimit detection. We conjecture that a similar effect may be observed in Minkowski space in a cavity with periodic boundary conditions, and may be harnessed in an experimental setup to better detect a UV cutoff of a field, or the shape of a qubit detector [37].

ACKNOWLEDGMENTS

This work was supported in part by the Natural Sciences and Engineering Research Council of Canada, and by the Asian Office of Aerospace Research and Development Grant No. FA2386-19-1-4077.

APPENDIX A: SHOWING THAT $|\alpha_{\ell m}\rangle$ IS A COHERENT STATE

In this section we will show that

$$|\alpha_{\ell m}\rangle = \hat{\mathcal{D}}_{\ell m}|0\rangle = \exp\left(\sum_{\ell,m}(\alpha_{\ell m}\hat{a}^\dagger_{\ell m} - \alpha^*_{\ell m}\hat{a}_{\ell m})\right)|0\rangle \tag{A1}$$

is a coherent state, i.e. that $|\alpha_{\ell m}\rangle$ is an eigenstate of the annihilation operator $\hat{a}_{ij}$.

Using the canonical commutation relation, $[\hat{a}_{ij},\hat{a}^\dagger_{\ell m}] = \delta_{i\ell}\delta_{jm}$, we can show that

$$\begin{aligned}\hat{a}_{ij}&\left(\sum_{\ell,m}(\alpha_{\ell m}\hat{a}^\dagger_{\ell m} - \alpha^*_{\ell m}\hat{a}_{\ell m})\right)\\ &= \alpha_{ij} + \left(\sum_{\ell,m}(\alpha_{\ell m}\hat{a}^\dagger_{\ell m} - \alpha^*_{\ell m}\hat{a}_{\ell m})\right)\hat{a}_{ij}\end{aligned} \tag{A2}$$

yielding

$$\left[\hat{a}_{ij}, \sum_{\ell,m}(\alpha_{\ell m}\hat{a}^\dagger_{\ell m} - \alpha^*_{\ell m}\hat{a}_{\ell m})\right] = \alpha_{ij} \in \mathbb{C} \tag{A3}$$

from which we find

$$\begin{aligned}[\hat{a}_{ij},\hat{\mathcal{D}}_{\ell m}] = &\left[\hat{a}_{ij}, \sum_{\ell,m}(\alpha_{\ell m}\hat{a}^\dagger_{\ell m} - \alpha^*_{\ell m}\hat{a}_{\ell m})\right]\\ &\times \exp\left(\sum_{\ell,m}(\alpha_{\ell m}\hat{a}^\dagger_{\ell m} - \alpha^*_{\ell m}\hat{a}_{\ell m})\right) = \alpha_{ij}\hat{\mathcal{D}}_{\ell m}.\end{aligned} \tag{A4}$$

Hence,

$$\hat{a}_{ij}|\alpha_{\ell m}\rangle = \hat{a}_{ij}\hat{\mathcal{D}}_{\ell m}|0\rangle = [\hat{a}_{ij}, \hat{\mathcal{D}}_{\ell m}]|0\rangle + \hat{D}_{\ell m}\hat{a}_{ij}|0\rangle = \alpha_{ij}|\alpha_{\ell m}\rangle \tag{A5}$$

showing that $|\alpha_{\ell m}\rangle$ is an eigenstate of the annihilation operator $\hat{a}_{ij}$ and so is a coherent state.

APPENDIX B: DERIVATION OF THE SPHERICAL HARMONICS COEFFICIENTS $g_{\ell m}$ FOR A GAUSSIAN DETECTOR ON $S^2 \times R$

The spherical harmonics coefficients $g_{\ell m}$ for the symmetric FB distribution (75) are given by

$$g_{\ell m} = \langle g(\kappa,\beta,\theta), Y_\ell^m\rangle = \int_0^\pi \int_0^{2\pi} \frac{e^{\kappa\cos(\theta)}}{C(\kappa,0)} Y_\ell^{m*}\sin(\theta)d\theta d\varphi = \frac{N_{\ell m}}{C(\kappa,0)}\int_0^\pi e^{\kappa\cos\theta}P_\ell^m(\cos\theta)\sin\theta d\theta$$
$$\int_0^{2\pi} e^{-im\varphi}d\varphi = 2\pi\delta_{m,0}\frac{N_{\ell 0}}{C(\kappa,0)}\int_0^\pi e^{\kappa\cos\theta}P_\ell^0(\cos\theta)\sin\theta d\theta = \delta_{m,0}\sqrt{\frac{2\ell+1}{4\pi}}\frac{2\pi}{C(\kappa,0)}\int_0^\pi e^{\kappa\cos\theta}P_\ell^0(\cos\theta)\sin\theta d\theta \tag{B1}$$

and using [41]

$$e^{\kappa\cos\theta} = \sqrt{\frac{\pi}{2\kappa}}\sum_{n=0}^{\infty}(2n+1)I_{2n+1/2}(\kappa)P_n^0(\cos\theta) \tag{B2}$$

we can rewrite the θ integral as

$$\begin{aligned} g_{\ell m} &= \sqrt{\frac{2\ell+1}{4\pi}}\frac{2\pi\delta_{m,0}}{C(\kappa,0)}\sqrt{\frac{\pi}{2\kappa}}\sum_{n=0}^{\infty}(2n+1)I_{n+1/2}(\kappa)\int_0^\pi P_n^0(\cos\theta)P_\ell^0(\cos\theta)\sin\theta d\theta \\ &= \sqrt{\frac{2\ell+1}{4\pi}}\frac{2\pi\delta_{m,0}}{C(\kappa,0)}\sqrt{\frac{\pi}{2\kappa}}\sum_{n=0}^{\infty}(2n+1)I_{n+1/2}(\kappa)\frac{2}{2n+1}\delta_{\ell,n} = \sqrt{\frac{2\ell+1}{4\pi}}\frac{4\pi\delta_{m,0}}{C(\kappa,0)}\sqrt{\frac{\pi}{2\kappa}}I_{\ell+1/2}(\kappa) \\ &= \delta_{m,0}\sqrt{\frac{2\ell+1}{4\pi}}\frac{4\pi\sqrt{\kappa}}{2\pi\sqrt{2\pi}I_{1/2}(\kappa)}\sqrt{\frac{\pi}{2\kappa}}I_{\ell+1/2}(\kappa) \equiv \delta_{m,0}\sqrt{\frac{2\ell+1}{4\pi}}\frac{I_{\ell+1/2}(\kappa)}{I_{1/2}(\kappa)} \\ &= \delta_{m,0}g_\ell. \end{aligned} \tag{B3}$$

For the squeezed FB distribution [Eq. 74], the spherical harmonics coefficients are given by

$$\begin{aligned} g_{\ell m} &= \int_0^\pi\int_0^{2\pi}\frac{e^{\kappa\cos\theta+\beta\sin^2\theta\cos 2\varphi}}{C(\kappa,\beta)}Y_\ell^{m*}\sin(\theta)d\theta d\varphi \\ &= \frac{N_{\ell m}}{C(\kappa,\beta)}\int_0^\pi e^{\kappa\cos\theta}P_\ell^m(\cos\theta)\sin\theta d\theta\times\int_0^{2\pi}e^{\beta\sin^2\theta\cos(2\varphi)-im\varphi}d\varphi \\ &= \frac{2\pi N_{\ell m}}{C(\kappa,\beta)}\int_0^\pi e^{\kappa\cos\theta}P_\ell^m(\cos\theta)\sin\theta d\theta(I_{m/2}(\beta\sin^2\theta)). \end{aligned} \tag{B4}$$

Now let $\cos(\theta) = z$, which allows us to rewrite the integral above as

$$g_{\ell m} = 2\pi\frac{N_{\ell m}}{C(\kappa,\beta)}\int_{-1}^1 e^{\kappa z}P_\ell^m(z)I_{m/2}(\beta(1-z^2))\,dz. \tag{B5}$$

APPENDIX C: THE POSITION INDEPENDENCE OF THE NONSIGNALING PART OF THE TRANSITION PROBABILITY

In this appendix we provide details of the simplification of the nonsignaling part of the transition probability.

The transition probabilities of the two detectors are

$$P_A = \frac{1}{2}[1 - \exp(-\alpha_A)] \tag{C1}$$

$$P_B = \frac{1}{2}[1 - \exp(-\alpha_B)\cos(2\Theta)], \tag{C2}$$

where Θ is the field commutator between detectors A and B defined in Eq. (54). We refer to α_D $(D \in \{A, B\})$ as the nonsignaling part of the transition probability because it does not depend on the properties of the other detector.

In general

$$\alpha_D = \sum_\ell \sum_{m=-\ell}^{\ell} |\alpha^D_{\ell,m}|^2, \tag{C3}$$

where

$$\alpha^D_{\ell,m} = -\frac{i\lambda_D \eta_D}{\sqrt{2\ell+1}} e^{i(\ell+1/2)T_D} f^D_{\ell,m} \tag{C4}$$

and $f^D_{\ell,m}$ are the spherical harmonic coefficients of the spatial profile of the detector D. Recall that these coefficients include the information about the location of the detector. Let $g^D_{\ell,m}$ be the spherical harmonic coefficients of detector D if it were located at the north pole and oriented along the $\varphi = 0$ axis, so that

$$f^D_{\ell,m} = \sum_{n=-\ell}^{\ell} D^\ell_{m,n}(\alpha,\beta,\gamma) g^D_{\ell,n}, \tag{C5}$$

where $D^\ell_{m,n}(\alpha,\beta,\gamma)$ are the Wigner-d functions. Now all the information about the position and orientation of the detector is encoded in the Euler angles α, β, and γ.

Substituting Eqs. (C4) and (C5) into the nonsignaling part [Eq. (C3)] yields

$$\begin{aligned}
\alpha_D &= \sum_\ell \sum_{m=-\ell}^{\ell} \left| -\frac{i\lambda_D \eta_D}{\sqrt{2\ell+1}} e^{i(\ell+1/2)T_D} \sum_{n=-\ell}^{\ell} D^\ell_{m,n}(\alpha,\beta,\gamma) g^D_{\ell,n} \right|^2 \\
&= \lambda_D^2 \eta_D^2 \sum_\ell \frac{1}{2\ell+1} \sum_{m=-\ell}^{\ell} \left| \sum_{n=-\ell}^{\ell} D^\ell_{m,n}(\alpha,\beta,\gamma) g^D_{\ell,n} \right|^2 \\
&= \lambda_D^2 \eta_D^2 \sum_\ell \frac{1}{2\ell+1} \sum_{n=-\ell}^{\ell} \sum_{n'=-\ell}^{\ell} g^D_{\ell,n} g^{D\,*}_{\ell,n'} \left(\sum_{m=-\ell}^{\ell} D^\ell_{m,n}(\alpha,\beta,\gamma) D^{\ell\,*}_{m,n'}(\alpha,\beta,\gamma) \right).
\end{aligned} \tag{C6}$$

The Wigner-d functions obey the orthogonality relations [47]

$$\sum_{m=-\ell}^{\ell} D^\ell_{m,n}(\alpha,\beta,\gamma) D^{\ell *}_{m,n'}(\alpha,\beta,\gamma) = \delta_{n,n'} \tag{C7}$$

$$\sum_{n=-\ell}^{\ell} D^{\ell *}_{m,n}(\alpha,\beta,\gamma) D^\ell_{m',n}(\alpha,\beta,\gamma) = \delta_{m,m'}, \tag{C8}$$

which we will now use to simplify Eq. (C6):

$$\begin{aligned}
\alpha_D &= \lambda_D^2 \eta_D^2 \sum_\ell \frac{1}{2\ell+1} \sum_{n=-\ell}^{\ell} \sum_{n'=-\ell}^{\ell} g^D_{\ell,n} g^{D*}_{\ell,n'} (\delta_{n,n'}) \\
&= \lambda_D^2 \eta_D^2 \sum_\ell \frac{1}{2\ell+1} \sum_{n=-\ell}^{\ell} |g^D_{\ell,n}|^2
\end{aligned} \tag{C9}$$

which does not depend the position and orientation of the detector.

Additionally, in the case of identical detectors ($\lambda_A = \lambda_B$, $\eta_A = \eta_B$ and $g^A_{\ell,m} = g^B_{\ell,m}$), then

$$\begin{aligned}
\alpha_A &= \lambda_A^2 \eta_A^2 \sum_\ell \frac{1}{2\ell+1} \sum_{m=-\ell}^{\ell} |g^A_{\ell,m}|^2 \\
&= \lambda_B^2 \eta_B^2 \sum_\ell \frac{1}{2\ell+1} \sum_{m=-\ell}^{\ell} |g^B_{\ell,m}|^2 = \alpha_B.
\end{aligned} \tag{C10}$$

APPENDIX D: THE SMEARED FIELD COMMUTATOR IN THE CASE OF UNSQUEEZED DETECTORS

In this section we provide details of the simplification of the smeared field commutator, Eq. (54), in the case of regular detectors.

If a detector is centered at the north pole of the sphere, and its smearing function is regular, i.e. it only depends on the angle θ, then its spherical harmonics coefficients can be written as

$$g_{\ell,m} = \delta_{m,0} g_\ell. \tag{D1}$$

If a regular detector is moved away from the north pole, then its spherical harmonics coefficients can now be written in terms of Wigner-d functions:

$$f_{\ell,m} = \sum_{n=-\ell}^{\ell} D^{\ell}_{m,n}(\alpha,\beta,\gamma)(\delta_{n,0} g_\ell) = D^{\ell}_{m,0}(\alpha,\beta,\gamma) g_\ell. \tag{D2}$$

Now consider two regular detectors, one centered at the north pole and the second centered at $(\theta,\varphi) = (\theta_B,\varphi_B)$. The smeared field commutator [Eq. (54) between can be simplified as

$$\begin{aligned}
[\hat{\mathcal{Y}}_A, \hat{\mathcal{Y}}_B] &= -\lambda_A\lambda_B\eta_A\eta_B \sum_{\ell,m} \frac{1}{2\ell+1} [(f^A_\ell \delta_{m,0})^* (D^{\ell}_{m,0}(\varphi_B,\theta_B,\gamma) g^B_\ell) \mathrm{e}^{\mathrm{i}(\ell+1/2)(T_B-T_A)} \\
&\quad - (f^A_\ell \delta_{m,0})(D^{\ell}_{m,0}(\varphi_B,\theta_B,\gamma) g^B_\ell)^* \mathrm{e}^{-\mathrm{i}(\ell+1/2)(T_B-T_A)}] \\
&= -\lambda_A\lambda_B\eta_A\eta_B \sum_{\ell=0}^{\infty} \frac{1}{2\ell+1} [f^{A^*}_\ell g^B_\ell D^{\ell}_{0,0}(\varphi_B,\theta_B,\gamma) \mathrm{e}^{\mathrm{i}(\ell+1/2)(T_B-T_A)} - f^A_\ell g^{B^*}_\ell D^{\ell}_{0,0}{}^*(\varphi_B,\theta_B,\gamma) \mathrm{e}^{-\mathrm{i}(\ell+1/2)(T_B-T_A)}] \\
&= -\lambda_A\lambda_B\eta_A\eta_B \sum_{\ell=0}^{\infty} \frac{1}{2\ell+1} \left[f^{A^*}_\ell g^B_\ell \left(\sqrt{\frac{4\pi}{2\ell+1}} Y^*_{\ell,0}(\theta_D,\varphi_D) \right) \mathrm{e}^{\mathrm{i}(\ell+1/2)(T_B-T_A)} \right. \\
&\quad \left. - f^A_\ell g^{B^*}_\ell \left(\sqrt{\frac{4\pi}{2\ell+1}} Y_{\ell,0}(\theta_D,\varphi_D) \right) \mathrm{e}^{-\mathrm{i}(\ell+1/2)(T_B-T_A)} \right] \\
&= -\lambda_A\lambda_B\eta_A\eta_B \sum_{\ell=0}^{\infty} \frac{1}{2\ell+1} \left[f^{A^*}_\ell g^B_\ell \left(\sqrt{\frac{4\pi}{2\ell+1}} \sqrt{\frac{2\ell+1}{4\pi}} P_\ell[\cos(\theta_B)] \right) \mathrm{e}^{\mathrm{i}(\ell+1/2)(T_B-T_A)} \right. \\
&\quad \left. - f^A_\ell g^{B^*}_\ell \left(\sqrt{\frac{4\pi}{2\ell+1}} \sqrt{\frac{2\ell+1}{4\pi}} P_\ell[\cos(\theta_B)] \right) \mathrm{e}^{-\mathrm{i}(\ell+1/2)(T_B-T_A)} \right] \\
&= -\lambda_A\lambda_B\eta_A\eta_B \sum_{\ell=0}^{\infty} \frac{1}{2\ell+1} [f^{A^*}_\ell g^B_\ell P_\ell[\cos(\theta_B)] \mathrm{e}^{\mathrm{i}(\ell+1/2)(T_B-T_A)} - f^A_\ell g^{B^*}_\ell P_\ell[\cos(\theta_B)] \mathrm{e}^{-\mathrm{i}(\ell+1/2)(T_B-T_A)}].
\end{aligned} \tag{D3}$$

[1] Achim Kempf, Gianpiero Mangano, and Robert B. Mann, Hilbert space representation of the minimal length uncertainty relation, Phys. Rev. D **52**, 1108 (1995).
[2] Sabine Hossenfelder, Minimal length scale scenarios for quantum gravity, Living Rev. Relativity **16**, 03 (2012).
[3] Achim Kempf, Quantum gravity, information theory and the CMB, Found. Phys. **48**, 1191 (2018).
[4] Achim Kempf, Spacetime could be simultaneously continuous and discrete, in the same way that information can be, New J. Phys. **12**, 115001 (2010).
[5] C. E. Shannon, A mathematical theory of communication, Bell Syst. Tech. J. **27**, 379 (1948).
[6] Achim Kempf and Robert Martin, Information Theory, Spectral Geometry, and Quantum Gravity, Phys. Rev. Lett. **100**, 021304 (2008).
[7] A. Kempf, A. Chatwin-Davies, and R. T. W. Martin, A fully covariant information-theoretic ultraviolet cutoff for scalar fields in expanding Friedmann Robertson Walker spacetimes, J. Math. Phys. (N.Y.) **54**, 022301 (2013).
[8] Aidan Chatwin-Davies, Achim Kempf, and Robert T. W. Martin, Natural Covariant Planck Scale Cutoffs and the Cosmic Microwave Background Spectrum, Phys. Rev. Lett. **119**, 031301 (2017).
[9] Laura J. Henderson, Robie A. Hennigar, Robert B. Mann, Alexander R. H. Smith, and Jialin Zhang, Harvesting entanglement from the black hole vacuum, Classical Quantum Gravity **35**, 21LT02 (2018).
[10] W. G. Unruh, Notes on black-hole evaporation, Phys. Rev. D **14**, 870 (1976).
[11] M O Scully, The time dependent Schrodinger equation revisited I: Quantum field and classical Hamilton-Jacobi routes to Schrodinger's wave equation, J. Phys. Conf. Ser. **99**, 012019 (2008).
[12] Laura J. Henderson and Nicolas C. Menicucci, Bandlimited entanglement harvesting, Phys. Rev. D **102**, 125026 (2020).
[13] Erickson Tjoa, Irene Ló pez-Gutiérrez, Allison Sachs, and Eduardo Martín-Martínez, What makes a particle detector click, Phys. Rev. D **103**, 125021 (2021).
[14] Benito A Juárez-Aubry and Jorma Louko, Onset and decay of the $1+1$ Hawking-Unruh effect: What the derivative-coupling detector saw, Classical Quantum Gravity **31**, 245007 (2014).

[15] Benito A. Juárez-Aubry and Jorma Louko, Quantum fields during black hole formation: How good an approximation is the Unruh state?, J. High Energy Phys. 05 (2018) 140.
[16] Bruno de S. L. Torres, T. Rick Perche, André G. S. Landulfo, and George E. A. Matsas, Neutrino flavor oscillations without flavor states, Phys. Rev. D **102**, 093003 (2020).
[17] T. Rick Perche, Caroline Lima, and Eduardo Martín-Martínez, Harvesting entanglement from complex scalar and fermionic fields with linearly coupled particle detectors, Phys. Rev. D **105**, 065016 (2022).
[18] Nadine Stritzelberger and Achim Kempf, Coherent delocalization in the light-matter interaction, Phys. Rev. D **101**, 036007 (2020).
[19] Nadine Stritzelberger, Laura J. Henderson, Valentina Baccetti, Nicolas C. Menicucci, and Achim Kempf, Entanglement harvesting with coherently delocalized matter, Phys. Rev. D **103**, 016007 (2021).
[20] Alejandro Pozas-Kerstjens and Eduardo Martin-Martinez, Harvesting correlations from the quantum vacuum, Phys. Rev. D **92**, 064042 (2015).
[21] Alejandro Pozas-Kerstjens and Eduardo Martin-Martinez, Entanglement harvesting from the electromagnetic vacuum with hydrogenlike atoms, Phys. Rev. D **94**, 064074 (2016).
[22] Richard Lopp and Eduardo Martín-Martínez, Quantum delocalization, gauge, and quantum optics: Light-matter interaction in relativistic quantum information, Phys. Rev. A **103**, 013703 (2021).
[23] Grant Salton, Robert B. Mann, and Nicolas C. Menicucci, Acceleration-assisted entanglement harvesting and range-finding, New J. Phys. **17**, 035001 (2015).
[24] Raúl Carballo-Rubio, Luis J. Garay, Eduardo Martín-Martínez, and José de Ramón, Unruh Effect Without Thermality, Phys. Rev. Lett. **123**, 041601 (2019).
[25] Laura J. Henderson, Robie A. Hennigar, Robert B. Mann, Alexander R. H. Smith, and Jialin Zhang, The BTZ black hole exhibits anti-Hawking phenomena, Phys. Lett. B **809**, 135732 (2020) .
[26] T. Rick Perche and Eduardo Martín-Martínez, Geometry of spacetime from quantum measurements, Phys. Rev. D **105**, 066011 (2022).
[27] T. Rick Perche and Ahmed Shalabi, Spacetime curvature from ultrarapid measurements of quantum fields, Phys. Rev. D **105**, 125011 (2022).
[28] Eduardo Martín-Martínez, Alexander R. H. Smith, and Daniel R. Terno, Spacetime structure and vacuum entanglement, Phys. Rev. D **93**, 044001 (2016).
[29] José Polo-Gómez, Luis J. Garay, and Eduardo Martín-Martínez, A detector-based measurement theory for quantum field theory, Phys. Rev. D **105**, 065003 (2022).
[30] Robert H. Jonsson, David Q. Aruquipa, Marc Casals, Achim Kempf, and Eduardo Martín-Martínez, Communication through quantum fields near a black hole, Phys. Rev. D **101**, 125005 (2020).
[31] Erickson Tjoa and Kensuke Gallock-Yoshimura, Channel capacity of relativistic quantum communication with rapid interaction, Phys. Rev. D **105**, 085011 (2022).
[32] Adam Teixidó-Bonfill, Alvaro Ortega, and Eduardo Martín-Martínez, First law of quantum field thermodynamics, Phys. Rev. A **102**, 052219 (2020).
[33] Petar Simidzija and Eduardo Martin-Martinez, Nonperturbative analysis of entanglement harvesting from coherent field states, Phys. Rev. D **96**, (065008 (2017).
[34] Stephen J. Summers and Reinhard Werner, Bell's inequalities and quantum field theory. II. Bell's inequalities are maximally violated in the vacuum, J. Math. Phys. (N.Y.) **28**, 2448 (1987).
[35] Bryce S. DeWitt, *Quantum Gravity: The New Synthesis* (Cambridge University Press, Cambridge, UK, 1980), pp. 680–745.
[36] Eduardo Martín-Martínez, Miguel Montero, and Marco del Rey, Wave packet detection with the Unruh-DeWitt model, Phys. Rev. D **87**, 064038 (2013).
[37] Emma McKay, Adrian Lupascu, and Eduardo Martín-Martínez, Finite sizes and smooth cutoffs in superconducting circuits, Phys. Rev. A **96**, 052325 (2017).
[38] Petar Simidzija and Eduardo Martin-Martinez, Harvesting correlations from thermal and squeezed coherent states, Phys. Rev. D **98**, 085007 (2018).
[39] Kensuke Gallock-Yoshimura and Robert B. Mann, Entangled detectors nonperturbatively harvest mutual information, Phys. Rev. D **104**, 125017 (2021).
[40] Gilad Lifschytz and Miguel Ortiz, Scalar field quantization on the $(2+1)$-dimensional black hole background, Phys. Rev. D **49**, 1929 (1994).
[41] Yibeltal F. Alem, Zubair Khalid, and Rodney A. Kennedy, Spherical harmonic expansion of Fisher-Bingham distribution and 3d spatial fading correlation for multiple-antenna systems, IEEE transactions on vehicular technology **65**, 5695 (2016) .
[42] Eugene Paul Wigner and J. J. Griffin, *Group Theory and its Application to the Quantum Mechanics of Atomic Spectra* (Academic Press, New York, USA, 1959).
[43] Jacques Hadamard, The problem of diffusion of waves, Ann. Math. **43**, 510 (1942).
[44] Patrick J. Roddy and Jason D. McEwen, Sifting convolution on the sphere, IEEE Signal Process. Lett. **28**, 304 (2021).
[45] Robert Jonsson, Eduardo Martín-Martínez, and Achim Kempf, Information Transmission Without Energy Exchange, Phys. Rev. Lett. **114**, 110505 (2015).
[46] Abhisek Sahu, Irene Melgarejo-Lermas, and Eduardo Martín-Martínez, Sabotaging the harvesting of correlations from quantum fields, Phys. Rev. D **105**, 065011 (2022).
[47] J. Pagaran, S. Fritzsche, and G. Gaigalas, Maple procedures for the coupling of angular momenta. IX. Wigner D-functions and rotation matrices, Comput. Phys. Commun. **174**, 616 (2006).